FLOW VISUALIZATION STUDIES OF THE XFV-12A

Charles Lewis Peterson

NAVAL POSTGRADUATE SCHOOL
Monterey, California

THESIS

FLOW VISUALIZATION STUDIES
OF THE XFV-12A

by

Charles Lewis Peterson

March 1975

Thesis Advisor: A. E. Fuhs

Approved for public release; distribution unlimited.

UNCLASSIFIED

SECURITY CLASSIFICATION OF THIS PAGE (When Data Entered)

REPORT DOCUMENTATION PAGE

READ INSTRUCTIONS BEFORE COMPLETING FORM

1. REPORT NUMBER	2. GOVT ACCESSION NO. / 3. RECIPIENT'S CATALOG NUMBER
4. TITLE (and Subtitle): Flow Visualization Studies of the XFV-12A	5. TYPE OF REPORT & PERIOD COVERED: Master's Thesis; March 1975
	6. PERFORMING ORG. REPORT NUMBER
7. AUTHOR(s): Charles Lewis Peterson	8. CONTRACT OR GRANT NUMBER(s)
9. PERFORMING ORGANIZATION NAME AND ADDRESS: Naval Postgraduate School, Monterey, California 93940	10. PROGRAM ELEMENT, PROJECT, TASK AREA & WORK UNIT NUMBERS
11. CONTROLLING OFFICE NAME AND ADDRESS: Naval Postgraduate School, Monterey, California 93940	12. REPORT DATE: March 1975 / 13. NUMBER OF PAGES: 92
14. MONITORING AGENCY NAME & ADDRESS (if different from Controlling Office): Naval Postgraduate School, Monterey, California 93940	15. SECURITY CLASS. (of this report): Unclassified / 15a. DECLASSIFICATION/DOWNGRADING SCHEDULE

16. DISTRIBUTION STATEMENT (of this Report)

Approved for public release; distribution unlimited.

17. DISTRIBUTION STATEMENT (of the abstract entered in Block 20, if different from Report)

18. SUPPLEMENTARY NOTES

19. KEY WORDS (Continue on reverse side if necessary and identify by block number)

Recirculation
Reingestion
XFV-12A
Vortex Shedding

20. ABSTRACT (Continue on reverse side if necessary and identify by block number)

The XFV-12A incorporates thrust augmentation to generate propulsive lift. Under the influence of forward flight the lift jets are subject to bending, which produces shed vortices that induce velocities at the aircraft. Additionally, operations in ground effect during hover and for small forward velocities can result in reingestion of engine exhaust gases. The objectives of this thesis were twofold. The

DD FORM 1 JAN 73 1473 (Page 1) EDITION OF 1 NOV 65 IS OBSOLETE S/N 0102-014-6601

UNCLASSIFIED

SECURITY CLASSIFICATION OF THIS PAGE (When Data Entered)

Block #20 continued

first was to investigate analytically aspects of the vortex shedding phenomenon through the application of potential flow around the lifting surfaces of the aircraft. Secondly, experimental analysis was performed to determine the unique reingestion properties of the XFV-12A operating statically under various wing and canard configurations.

The pressure coefficient for jet curvature obtained under two-dimensional potential flow was 8.66. Reingestion of exhaust gases was primarily through the main inlet and not the auxiliary inlet; the source of most of the exhaust gas was the canard.

Flow Visualization Studies of the XFV-12A

by

Charles Lewis Peterson
Second Lieutenant, United States Marine Corps
B.S.A.E., United States Naval Academy, 1973

Submitted in partial fulfillment of the
requirements for the degree of

MASTER OF SCIENCE IN AERONAUTICAL ENGINEERING

from the

NAVAL POSTGRADUATE SCHOOL
March 1975

ABSTRACT

The XFV-12A incorporates thrust augmentation to generate propulsive lift. Under the influence of forward flight the lift jets are subject to bending, which produces shed vortices that induce velocities at the aircraft. Additionally, operations in ground effect during hover and for small forward velocities can result in reingestion of engine exhaust gases. The objectives of this thesis were twofold. The first was to investigate analytically aspects of the vortex shedding phenomenon through the application of potential flow around the lifting surfaces of the aircraft. Secondly, experimental analysis was performed to determine the unique reingestion properties of the XFV-12A operating statically under various wing and canard configurations.

The pressure coefficient for jet curvature obtained under two-dimensional potential flow was 8.66. Reingestion of exhaust gases was primarily through the main inlet and not the auxiliary inlet; the source of most of the exhaust gas was the canard.

TABLE OF CONTENTS

LIST OF ILLUSTRATIONS

Figure

LIST OF SYMBOLS

Symbol	
$\underline{A}$	Matrix of difference equation coefficients
A_1	Aerosol tube exit area
A_2	Canard primary air exit area
A_4	Main inlet entrance region area
A_m	Blower exit area
A_M	Manometer tube area
A_p	Leak detector probe inlet area
$\underline{B}$	Vector of boundary values
C_L	Pressure coefficient across jet
D	Canard reference length
E	Electric field
e_o	Permittivity constant
F	Percentage of freon ingested that leaves canard diffuser
F_1	Freon concentration in probe at moderate conditions
F_2	Freon concentration in diffuser
G	Percentage of inlet mass flow that is recirculated canard exhaust
H	Heavy reingestion
L	Height above ground measured from leading edge of canard
M	Moderate reingestion
$\dot{m}_o$	Reference leak mass flow rate
$\dot{m}_1$	Aerosol can mass flow rate
$\dot{m}_2$	Canard augmentor mass flow rate

Symbol	
$\dot{m}_3$	Leak detector probe mass flow rate
$\dot{m}_4$	Main inlet mass flow rate
n	Normal direction
P	Static pressure
q_∞	Dynamic pressure at freestream conditions
q_4	Dynamic pressure at main inlet
q_m	Dynamic pressure at blower exit plane
R_{ij}	Radius of curvature of streamtube
T	Trace reingestion
U_1	Velocity of freon from aerosol can
U_2	Velocity of primary air
U_4	Velocity of flow in main inlet
U_M	Velocity of manometer fluid
U_m	Velocity of expelled air at blower exit plane
U_p	Velocity of air ingested by detector probe
V	Voltage
W	Weak reingestion
$\underline{x}$	Vector of unknown stream function values
Γ	Circulation
θ	Angle between chord of canard or wing and ground
ρ	Electric charge density
ρ_a	Density of air at sea level, 70°F
ρ_f	Density of saturated freon vapor at 70°F
ϕ	Potential function
ψ	Stream function

ACKNOWLEDGEMENT

The author expresses his sincere appreciation to Distinguished Professor Allen Fuhs of the Department of Aeronautics, Naval Postgraduate School, Monterey, California, for his guidance and assistance. Sincere appreciation is also extended to Mr. Ronald Ramaker for his effort in modification of the model.

I. INTRODUCTION

The XFV-12A is a V/STOL aircraft currently under development by the Columbus Aircraft Division of North American Rockwell. Its design incorporates high performance supersonic operation in a fighter or attack mission as well as vertical and short take-off operations from proposed ships of the 1980's. A unique property of the XFV-12A is incorporation of thrust augmentation when operating under propulsive lift. Combining the effects of hypermixing nozzles and Coanda blowing, this aircraft is designed to take off vertically with a thrust-to-weight ratio of less than one. When it becomes operational, the XFV-12A will offer the first employment of thrust augmentation in military or civilian aircraft.

Problem areas under investigation include the shedding of vortices from the exhaust jets and an experimental analysis of the XFV-12A's recirculation properties. The vortex shedding phenomenon occurs when a downflow of the lift jets is modified by forward velocity, ground effect, or both. The resultant vortices are shed as a result of a bending of the lift jets as shown hypothetically in Figure 1. This bending is derived from a high pressure area underneath and a low pressure area above the jet. These vortices are generated in much the same manner as wing tip vortices produced in finite airfoil theory. The nature and influence of these vortices are the unknowns under investigation.

A potential flow solution to a propulsive lift system was performed by Albers and Potter in 1971 [Ref. 1]. This analysis assumed an exhaust profile in accordance with Spence's theory [Ref. 2] for a jet augmented flap. The McDonnell Douglas Corporation [Ref. 3] has conducted work on a jet-wing lifting surface theory using elementary vortex distributions. A solution for the exhaust profile itself, however, is not known.

The vortex shedding is a consequence of the pressure difference on the two sides of a bent jet. To gain insight into the vortex problem, a potential flow model was formulated to determine jet bending. The potential flow was solved by two methods. A computer program was used to solve Laplace's equation for two-dimensional potential flow. For this case, only the canard's influence was considered. A continuous solution was obtained using an electrostatic analogy. Conducting paper provided the flow domain. Laplace's equation was again applied, but under the influence of both the wing and canard in a two-dimensional analysis.

Recirculation experiments provide valuable data which adequately depict the reingestion properties of the XFV-12A. Since this characteristic is not readily calculated, results are based purely on experimental work performed and the current literature available on the subject. In subsequent discussions, the terms reingestion and recirculation will be used to describe the same phenomenon.

Considerable work has been performed in the area of recirculation properties of lift engines. Investigations

of recirculation for lift engines of various configurations applied to various airframe shapes have been performed [Refs. 4,5]. An analysis to determine the applicability of small scale testing has been done [Ref. 6]. Reduction of reingestion was examined by applying several concepts to prevent recirculated gases from entering lift engine inlets [Ref. 7]. Conclusions have not always been consistent when analyzing the most significant contribution to recirculation or the optimal method of prevention. However, it was commonly held that reingestion is a unique property for each airframe and accompanying engine configuration. Thus the particular properties of the XFV-12A operating in the vertical or short take-off mode offer a unique problem.

The reingestion problem was investigated experimentally. The literature was helpful in formulating and designing experimental apparatus and procedures. For carrying out the experiments, a one-tenth scale semi-span model of the XFV-12A was used. In order to simulate a zero forward velocity, testing was performed statically. Recirculation properties of interest included results for both the STOL and VTOL configurations at varying heights above the ground. In all cases, the reingestion at both the main and auxiliary inlets was determined.

The computer program and its background are discussed in Section II of this thesis. Section III contains the work done with the electrostatic analogy. The next section describes the arrangement of the experimental apparatus including supplemental hardware necessary to supply appropriate simulation of

the lift engines. Section V covers experimental work performed preliminary to the actual reingestion tests. The reingestion experiments are described in Section VI. Experimental results, conclusions, and recommendations follow. Graphical test results and test data are recorded subsequent to the text.

II. COMPUTER SOLUTION TO THE POTENTIAL FLOW EQUATIONS FOR TWO-DIMENSIONAL THRUST AUGMENTOR CANARD

A. ASSUMPTIONS

In formulating the problem, the mass flow rate of the air leaving the diffuser exit plane was assumed to be equal to the secondary air entering the diffuser. This assumption was essential for satisfying continuity in the control volume which encircled the canard. (Using an experimentally obtained augmentation ratio of 6.84 [Ref. 8], the actual ratio of exhaust at the canard exit to the secondary flow is about eight to seven.)

The working fluid was assumed to be incompressible, irrotational, and two-dimensional. With the irrotationality assumption, Euler's equations of motion for fluids become homogeneous. When a single dependent variable representing the potential function is introduced, a single partial differential equation results.

$$\frac{\partial^2 \phi}{\partial x^2} + \frac{\partial^2 \phi}{\partial y^2} = 0. \qquad (1)$$

The conjugate function to the potential function, or the stream function, is derived from the continuity equation for incompressible flow.

$$\frac{\partial^2 \psi}{\partial x^2} + \frac{\partial^2 \psi}{\partial y^2} = 0. \qquad (2)$$

The equation for the stream function was solved in the computer program.

B. NATURE OF PROBLEM

The equation for the stream function is elliptical in nature yielding a boundary value problem. The boundary conditions were of the Dirichlet type. Values of the stream function were specified on all edges of the domain. Values of the stream function were also assigned to the canard flaps [Ref. 9]. The boundary conditions were held constant on the upper and lower bounds. The rate of change of stream function values on the upstream and downstream boundaries was held constant. These boundary conditions duplicated freestream conditions.

For simplicity, only the canard was considered in this analysis. It was positioned nine chord lengths from the front boundary of the domain to its leading edge. The rear of the domain was positioned about 40 chord lengths aft of the canard. At this position it was anticipated that the flow field disturbances generated by the canard would have returned to freestream conditions at the boundaries. The discretized domain is illustrated in Figure 2.

C. DISCRETIZATION

Since the canard is small compared to the size of the domain, a variable mesh was necessary to represent optimally the flow while economizing on computer storage requirements. It was anticipated that the direction of the streamlines would be changing most rapidly in the vicinity of the canard. The highest concentration of solution points was then near the canard. The coarsest distribution of solution points was located near the corner most distant from the canard.

The final distribution of solution points within the domain resulted in 201 distinct points.

Using a Taylor series expansion, the differential equation can be reduced to a difference equation as illustrated in Appendix A. Each solution point is expressed in terms of the four points adjacent to it. The resultant error on transition to difference equations is of the fourth order. Deriving a difference equation for each solution point results in 201 simultaneous, linear, algebraic equations in 201 unknowns. In matrix form, the problem is easily stated as

$$\underline{A} \cdot \underline{x} = \underline{B} \qquad (3)$$

where $\underline{A}$ is the matrix of coefficients for the unknown values of the stream function, $\underline{x}$ is the vector of unknown solution points, and $\underline{B}$ is a vector containing the boundary conditions assigned to both the perimeter of the domain and the canard flaps.

Since most of the elements in $\underline{A}$ are zero, it became more efficient to utilize a subroutine requiring only the storage of the nonzero elements and as few zero elements as possible. Such a library subroutine in the IBM 360 system at the Naval Postgraduate School is "GELB." This subroutine employs Gaussian elimination techniques in solving a banded matrix. This reduced the storage requirements for this particular problem by a factor of about ten. Not only did "GELB" reduce the time required to obtain a solution, but it provided for a finer mesh size within the domain for a given quantity of core space.

III. ELECTROSTATIC ANALOGY SOLUTION TO THE POTENTIAL FLOW EQUATION FOR A TWO-DIMENSIONAL THRUST AUGMENTOR WING AND CANARD SYSTEM

A. ELECTROSTATIC ANALOGY

The differential form of Gauss' flux theorem as it governs electric fields states that the divergence of the field is proportional to the charge density [Ref. 10]. In vector notation:

$$\nabla \cdot E = \rho / e_o . \tag{4}$$

Since the electric field, E, at any point is equal to the negative of the gradient of the electric potential, V,

$$E = - \nabla V . \tag{5}$$

Gauss' flux theorem can be rewritten as Poisson's equation.

$$\nabla^2 V = -\rho / e_o . \tag{6}$$

If Poisson's equation is assumed to apply in a region of zero charge density, the expanded two-dimensional electric potential equation can be written:

$$\frac{\partial^2 V}{\partial x^2} + \frac{\partial^2 V}{\partial y^2} = 0 . \tag{7}$$

This equation is Laplace's equation as it applies to electric fields [Ref. 10].

If the voltage is allowed to be proportional to the stream function, a plot of equipotential lines on some conducting medium will yield a continuous solution for the stream function [Ref. 11]. Additionally, the zero charge

density assumption is appropriate since it is analogous to the irrotationality requirement of potential flow.

Similarly, the current flowing in the domain is analogous to the fluid potential function. Since circulation is related to the potential function by

$$\Gamma = \int_C d\phi \qquad (8)$$

the value of the current can be used to measure circulation [Ref. 11].

B. EXPERIMENTAL APPARATUS

The hardware necessary to provide such a solution included conducting paper of a known resistance, an electrometer for use in measuring voltages and currents, a ten-volt d-c power source, and seven potentiometers (Figure 3). The potentiometers took a predesignated fraction of the ten-volt source and applied it to a particular component of the wing-canard system. A special pen which contained a conducting paint was used to draw the wing and canard onto the conducting paper.

The resistance of the paper was determined using a known voltage source and the electrometer which measured current. The electrometer was placed in series with the conducting paper and the voltage source. The resistance was measured to be approximately 10,000 ohms per centimeter. The potentiometers were selected so that their resistances would be much less than that of the paper, but large enough to keep a low amount of current flowing from the ten-volt source.

If the maximum allowable current in the battery was constrained to be ten milliamps, then the potentiometers had to be on the order of 1,000 ohms. This satisfied both the current and resistance constraints.

The voltage induced on the wing and canard flaps were assigned so as to provide for equal circulation around the forward and aft flaps of the wing and canard. In addition, voltages were constrained to provide a flow velocity in the canard and wing augmentors which was twice that of freestream conditions.

The equal circulation requirement was implemented by providing equal but opposite current flowing in the two Coanda flaps. The flow velocity constraint was imposed by comparing the distance between the Coanda flaps on the paper with the distance between the streamlines upstream which stagnated on those Coanda flaps.

The center ejector flaps were constrained to have zero current and a voltage value midway between those assigned to the Coanda flaps. These requirements resulted in a negligible lift contribution made by the center ejectors as well as an equal distribution of wing and canard augmentor inlet flow on each side of the center ejector.

In conducting the experiment, however, the equal-but-opposite circulation requirement could be imposed on the canard only. The results shown in Figure 4 indicate the streamlines having the same voltage value as those induced on the wing and canard flaps. The ground is the only portion of the boundary depicted.

IV. EXPERIMENTAL DESIGN AND MODEL MODIFICATION

A. PLUMBING AND FIXTURES

Compressed air was supplied by two compressors rated at 17.2 and 49.5 cubic feet per minute, respectively. One was equipped with a 100 gallon storage tank, while the other had an 80 gallon tank. These compressors were installed in parallel with three additional storage tanks with a capacity of 400 gallons each. The total storage capacity of the system was 1,380 gallons or 181.3 cubic feet.

The compressors were limited by design to a pressure of 137 lb/in^2. The actual operating pressure of the system was constrained to be no more than 125 lb/in^2. For the planned operating velocity at the ejectors of 136 ft/sec, substantially more than 15 minutes of experimental run time at the desired operating conditions was available.

A single regulator and stop valve connected the storage tanks to the plenum, which supplied the ejector hypermixing nozzles and Coanda blowing. This provided for single-valve control of the experiments. Once the desired pressures had been obtained by altering the setting on the plenum valves, the plenum valve settings could be held constant. Only the stop valve was needed to initiate and terminate a particular experimental run.

In anticipation of testing in the Naval Postgraduate School smoke tunnel, a two-inch pipe was channeled to the vicinity of the smoke tunnel from the storage tanks. In parallel with the outlet in the static testing area, the

pipe routed to the smoke tunnel was sealed during static testing. Simple transition to smoke tunnel testing can be performed by sealing the outlet in the static testing area and moving the regulator and stop valves to the smoke tunnel outlet.

The plenum has eight outlets of which only six are needed to supply the ejectors on the wing and canard. Three-quarter-inch-diameter automotive heater hoses were used to connect the plenum to the Coanda slots for both wing and canard. One-inch hoses were needed for both center ejectors (Fig. 5).

B. INLET SIMULATION

In order to depict adequately aircraft operation in the static position, some means of duplicating the effect of the inlets needed to be accomplished. Upon commencing work on the XFV-12A, only the main inlet had been fabricated with no means of providing suction for inlet flow.

The auxiliary inlet was fashioned from copper sheet metal and attached to the top of the aircraft model as shown in Figure 6. For both the main and auxiliary inlets, ducts were constructed for the purpose of establishing the correct inlet flow rate. The ducts are shown in Figure 7. A sufficient quantity of inlet flow is pumped to satisfy the continuity equation as applied to inlet and exit conditions. Continuity required that the sum of the mass flow rates entering the main and auxiliary inlets was equal to the mass flow rate of primary air from the wing and canard. (For

purposes of these experiments, the contribution of fuel to the mass flow rates of the exhaust jets was assumed to be negligible.)

A first attempt at entraining ambient air through the inlets was done using the ejector principle. Copper tubing with six ejectors was fabricated to blow air along the main inlet channel near the face of the inlet. A photograph of the ejector appears in Figure 9. A similar copper ejector was constructed for the same purpose in the auxiliary inlet. These ejectors were found to function but could not provide sufficient mass flow to match that leaving the Coanda slots and ejectors of the propulsive system. Thus, some other means of duplicating the suction effect at the inlets had to be devised.

A suction blower was attached to the inlet channels and sealed so that all of the entrained air was expelled out the exit plane of the blower; see Figure 10. Using this method the dynamic pressure measured at the exit plane of the blower was found to be 0.6 inches of water. For purposes of analysis of the continuity equation, the flow was assumed to be incompressible between the exit plane of the blower and the inlets. With this simplification, velocities and corresponding dynamic pressures at the inlet and the blower exit plane were dependent only on the relative areas.

$$U_4 A_4 = U_m A_m \tag{9}$$

and

$$\frac{q_4}{q_m} = \left[\frac{U_4}{U_m} \right]^2 = \left[\frac{A_m}{A_4} \right]^2. \tag{10}$$

The dynamic pressure at the exit plane of the motor dictates the conditions which must exist at the ejectors for continuity to be satisfied for the system.

Upon comparison of geometries, the required velocity at the main inlet was found to be 27.5 ft/sec. The correct velocity at the ejectors and Coanda slots of the wing and canard was then 136 ft/sec. Applying the augmentation ratio determined previously, the mean velocity at the exit plane of the diffusers must be 26.8 ft/sec.

C. MODEL MOUNTING

Once the inlets had been constructed, the model was mounted on three-quarter-inch plywood so that a plane of symmetry was established for testing purposes. The plane of symmetry is commonly known as a reflection plane. The other side of the reflection plane was cut away at the interior of the model to allow for the introduction of air from the plenum. A photograph of the reflection plane mounting at the static testing site is shown in Figure 8.

The ground was simulated by another piece of plywood mounted perpendicular to the model plane of symmetry and parallel to the ground. This piece was attached to the reflection plane with bolts and could be moved up and down with respect to the aircraft at one-inch intervals. The upper limit was analogous to placing the aircraft on the ground with the gear lowered. The lower limit simulated the aircraft at an altitude of 20 feet and was accomplished by removing the ground plane entirely.

As the "ground" was moved down from the aircraft during testing, it became necessary to use a larger piece of plywood to compensate for the enlarged area which was under the influence of the aircraft's exhaust jets. This was done by placing a larger piece of plywood covering 32 square feet directly over the original "ground."

V. PRELIMINARY EXPERIMENTAL WORK AND ANALYSIS

A. NATURE OF RECIRCULATION

Reingestion of hot exhaust gases is a problem of particular interest to designers of VTOL aircraft and STOL aircraft when operating at forward speeds of less than 25 knots [Ref. 12]. This phenomenon involves the entrainment of some portion of one or more exhaust jets into the intakes of the lift engines. Adverse effects on performance include a decrease in the available thrust, large increase in inlet temperature, and distortion in the temperature profile at the inlets [Ref. 7]. These last two effects can lead to stalling of the compressor and engine surge [Ref. 7]. Vertical takeoff and landing operations over areas with loose terrain also pose a problem of ingestion of particles kicked up by the exhaust jets [Ref. 13]. Potential loss of available control power was illustrated dramatically by a XC-142. A landing accident in 1965 was attributed to a loss in control power due to recirculation of hot exhaust gases [Ref. 12].

Exhaust gas reingestion has been classified according to the method in which exhaust gas is transported to the vicinity of the inlet. The first type is a diffusion of the exhaust gases into the ambient air. The buoyant force of the low density exhaust carries it up from the ground to the vicinity of the inlet. This is commonly called the "buoyant" effect [Ref. 5].

The second type of recirculation involves an interaction of the exhaust jets with the ground and subsequently with one another so that exhaust gases are forced upward in a "fountain" effect between the two exhaust jets. This type usually requires less time for its effects to be felt. The fountain effect usually is considered to be the most serious of the two types in terms of potential hazard to aircraft operation [Ref. 5].

The reingestion problem is one which cannot be treated analytically at present. Rather, experimental results are the only reliable source of information concerning the recirculation characteristics of a particular airframe shape and engine configuration. Even the interpretation of results has resulted in conflicting conclusions. For example, independent tests arrived at opposite conclusions with regard to the most significant type of reingestion transport [Refs. 5,7].

B. ANALYSIS OF VALIDITY OF SMALL-SCALE TESTING

In order for experimental results to be valid, reingestion characteristics observed for the scale model must be applicable to the full-scale aircraft. Also, since operating conditions of the aircraft may differ from those imposed on the model during testing, reingestion must be evaluated as a function of differing exit temperature and pressure conditions.

In an investigation of scaling effects on VTOL recirculation, recirculation was determined to be scalable both

statically and dynamically [Ref. 6]. (The experimental variables used were temperature, temperature gradient, and inlet distortion.) Another analysis determined reingestion to be independent of the temperature and pressure profiles exhibited by the engine over the range tested [Ref. 4]. These conclusions indicated that the experimental test conditions provided significant results even though full scale operating conditions were not duplicated.

With specific regard to the XFV-12A, an evaluation of the characteristics of thrust augmentation indicated that the augmentation ratio of a system is almost independent of nozzle pressure ratio [Ref. 14]. Consequently, conditions unique to propulsive lift employing thrust augmentation were duplicated at the test conditions.

C. SMOKE AND LASER TESTING

The first experiments performed to determine the existence of recirculating exhaust gases were done using smoke introduced into the flow and a portable laser for detection. A smoke jet was produced from an oil smoke generator similar to those used in the NPS smoke tunnel. Using an air flow from one of the extra outlets of the operating plenum, the smoke was forced through a narrow length of plastic tubing to the vicinity of the canard ejector.

The smoke was laminar for about 2 or 3 inches upon leaving the tube, followed by transition to turbulence as it was entrained with secondary air into the canard. Subsequent to entrainment the smoke was impossible to trace without the use of the laser.

The smoke experiments were successful in demonstrating a small degree of recirculation, although no quantitative results could be determined. They also demonstrated that the main and auxiliary inlet ejectors functioned as desired but were unable to develop sufficient amounts of inlet flow to match the wing and canard ejectors. The results of smoke testing were inconclusive; however, the results did indicate that further investigation was desirable.

D. EXPLORATORY FREON TESTING

Experiments conducted in similar fashion to the smoke tests were performed using an aerosol can containing freon instead of smoke. A freon leak detector normally used to detect refrigerant leaks was used to measure reingestion.

These results confirmed that exhaust gases were being reingested, though there was again inadequate suction at both intakes. This experiment demonstrated the need for a better method of inlet simulation as well as further analysis of reingestion characteristics.

VI. REINGESTION EXPERIMENTS

A. DESCRIPTION OF LEAK DETECTOR

As a detection device, a General Electric refrigerant leak detector was acquired. Normally used to detect leaks as small as 1/2 oz/yr in coolant systems, it was aptly suited for use in detecting exhaust gases contaminated with freon. The detector is illustrated in Figure 11.

The sensitivity of the detector was varied by a knob on the face of the instrument and by a switch which indicated either a high or low sensitivity setting. The probe held a light which flashed when freon was absorbed. The flash rate gave a qualitative indication of the absorption rate, although the flash frequency was not proportional to the freon contamination of the mass flow being absorbed.

A moderate rate of reingestion was defined as that flash frequency which was equal to that obtained when the probe was placed directly over the reference leak. Since the reference leak has a known mass flow rate, it can be used as a reference value. Three other ordinal quantitative descriptions, heavy, light, and trace, were used to represent deviations from the reference "moderate" condition.

Before each experimental run, the detector was adjusted by reducing or increasing the sensitivity until at free-stream conditions, the probe light just ceased to flash. Thus each set of data was acquired using the same reingestion descriptions. Contamination of the ambient air at low

levels of freon forced experiments to be performed at substantial time intervals. This allowed the background freon contamination to dissipate and provided time to resupply the compressed air storage tanks.

B. EXPERIMENTAL DEPENDENT VARIABLES

Of interest in performing the experiments was the flow path of recirculating gases from the exit plane of the diffuser of both the canard and wing to the main and auxiliary inlets. It was anticipated that these recirculation characteristics would vary with height above the ground and with the angle between the chord of the wing and canard flaps and the ground. The investigation covered recirculation characteristics as height above the ground varied from zero to about 24 inches (20 feet in full-scale dimensions). The angle of the canard and wing flaps was varied for each height at 10 degree increments from the vertical to an angle of 30 degrees from the vertical. Thus the pattern of reingestion was investigated for the aircraft operating in both the STOL and VTOL modes.

In addition, a profile of the distribution of recirculated exhaust at the main inlet was determined. This was done by converting the six main inlet ejectros previously employed unsuccessfully to the role of gas sampling ports. Tests were performed at a height above ground of zero and with the wing and canard flaps in the VTOL configuration only. Profiles were acquired which reflected the distribution of exhaust gases from the front or rear Coanda slots or the ejector in the canard.

C. QUANTITATIVE REINGESTION ANALYSIS

Some means were necessary of quantitatively specifying the meaning of the descriptions of degree of reingestion. Since the term "moderate" has been assigned to that amount of intake corresponding to the reference leak, it provided the only basis for a quantitative analysis.

A result can be obtained analytically in a straightforward manner if some assumptions are made concerning the conditions under which the experiments were conducted and the nature and properties of the freon. First, it was assumed that thermodynamic properties could be evaluated at 70°F. The freon was assumed to have the molecular weight of Freon-12 (CCl_2F_2); see [Ref. 15]. The freon in the aerosol can was assumed to be a mixture of vapor and liquid at saturation conditions.

Five mass flow rates must be calculated using known properties of freon and air and the previously outlined assumptions. The mass flow rate of freon from the reference leak is required; this is equal to the mass flow rate for moderate recirculation. The mass flow rate of air in the diffuser was also needed, as well as the mass flow rate of the detection probe. Finally, the mass flow rates of the inlets and the aerosol can were calculated. The various mass flow rates and corresponding sources and sinks are diagramatically shown in Figure 12.

The mass flow rate of the reference leak is known to be 1/2 oz/yr from the instructions for use of the instrument. When the units are altered to yield lbm/sec, the result is

$$\dot{m}_o = 0.99 \times 10^{-9} \text{ lbm/sec.}$$

The mass flow rate of the aerosol can was resolved using the momentum conservation equation and solving for velocity.

$$U_1^2 = \frac{2(\Delta P)}{\rho_f} . \qquad (11)$$

The pressures and density were obtained from a table of properties of saturated freon [Ref. 15]. The calculated velocity is

$$U_1 = 567 \text{ ft/sec.}$$

The diameter of the tube leading from the aerosol can was measured to be 0.025 inches. The mass flow rate was then readily calculated.

$$\dot{m}_1 = 3.92 \times 10^{-3} \text{ lbm/sec.}$$

The mass flow rate in the diffuser was computed using the results obtained for the augmentation ratio [Ref. 8] and the exit conditions of the wing and canard diffusers. Using a primary air velocity of 136 ft/sec, the mass flow rate of the canard diffuser is

$$\dot{m}_2 = 4.58 \times 10^{-1} \text{ lbm/sec.}$$

The mass flow rate in the probe required a supplementary experiment. The probe was attached to a manometer at one end. The other end led to a reservoir of fluid whose upper surface was exposed to ambient conditions. For small changes in pressure, incompressibility can be assumed for the air. The flow rate of gas being drawn into the probe could be inferred by observing the rate of displacement of the manometer fluid.

Using the speed of the air in the manometer tube, the mass flow rate of the gas in the detector probe could be computed directly from the continuity equation for incompressible flow. Subsequent applications of these results assumed that air was the dominant gas being absorbed by the probe.

$$U_p A_p = U_M A_M. \tag{12}$$

Solving for the only unknown, U_p, yields a velocity of gas in the probe of 5.37 in/sec. The mass flow rate of the probe was

$$\dot{m}_3 = 4.82 \times 10^{-6} \text{ lbm/sec.}$$

The mass flow rate of the main inlet was calculated using measurements taken at the exit plane of the electric blower. The dynamic pressure was recorded which yielded the velocity at the blower exit. Comparing geometries from the analysis described in Section IVB, the properties at both inlets could be calculated. The resultant mass flow rate for the main inlet was

$$\dot{m}_4 = 6.29 \times 10^{-2} \text{ lbm/sec.}$$

The mass flow rate of the auxiliary inlet was assumed to be the same as that of the main inlet. The area of the auxiliary inlet is greater than that of the main inlet. However, two ducts of equal area connected the inlets to the blower. These ducts were smaller in cross sectional than either inlet and consequently dictated the mass flow rate of each.

The first problem in quantitative analysis was the computation of the fraction of mass flow in the detection probe that was freon. For a moderate reingestion rate, this was represented by the ratio of the mass flow rate in the reference leak to the mass flow rate of the probe.

$$F_1 = \dot{m}_o/\dot{m}_3 = 2.06 \times 10^{-4}.$$

The second problem was finding the concentration of freon in the diffuser of the canard. Since this concentration was assumed to be constant from the point of introduction to the ejector, it was found by computing the ratio of mass flow rate of freon introduced into the air hose to the mean flow rate of air at the exit plane of the diffuser.

$$F_2 = \dot{m}_1/\dot{m}_2 = 8.58 \times 10^{-3}.$$

A reingestion percentage was then calculated yielding the concentration of freon being ingested as compared to that being expelled. For moderate reingestion conditions

$$F = F_1/F_2 = 2.40\%.$$

Consequently a moderate reading indicated that 2.40% of the diffuser exit mass flow was being reingested by the main inlet.

Further, it was desirable to know the percentage of inlet flow that was recirculated from the engine exhausts. This was computed simply by multiplying the reingestion percentage by the mass flow rate of the diffuser, then dividing by the mass flow rate of the main inlet.

$$G = F \times \dot{m}_2/\dot{m}_4 = 17.8\%.$$

Therefore a moderate reingestion reading indicated that about 18% of the inlet flow was comprised of recirculated exhaust gases. Here exhaust gases were defined as the mixture of entrained secondary air and primary air expelled from the canard or wing augmentor.

D. EXPERIMENTAL PROCEDURE

Freon was injected through drilled holes in the heater hoses leading to the Coanda slots and the ejectors. The aerosol can could be moved readily to introduce freon into any given flap. The six points of introduction were assigned station numbers sequentially from the forwardmost canard flap aft. The flaps and their accompanying station numbers are shown in Figure 13. Holes were drilled in the ducts leading from the inlets to which the detector probe was attached. The wing and canard flaps were set by measuring the angle between the chord of each flap and the vertical. The stiffness of the hoses was sufficient to maintain the position of the wing and canard flaps throughout a set of experiments.

The experiments were conducted by varying the height above the ground with a constant wing and canard angle. Measurements were taken at both the main and auxiliary inlets for each of the six points of introduction. Thus twelve readings were taken at each height above the ground for each wing and canard angle. The wing and canard were rotated together, so that there were no experimental runs for which the wing and canard angles were different. A total of 288 reingestion readings were taken.

The results were plotted according to the twelve combinations of inlet and point of introduction. The twelve reingestion profiles are shown in Figures 14-25. The abscissa of each graph is the angle between the chord of the wing and canard flaps and the ground. The ordinate is the height above the ground, non-dimensionalized with respect to a canard reference length. The canard reference length was defined as the square root of the area of the entrance plane of the canard augmentor. Its value is 4.90 in.

The experiments covering the inlet reingestion profile were performed with the canard since the wing did not contribute substantially to main inlet recirculation. Five of the six different gas sampling ports in the inlet face were sealed with adhesive tape at any one time, so that the reingestion reading measured only streamtubes passing near the open port. The response of all six sampling ports on the inlet face was recorded for each of the three points of introduction. A total of 18 readings were taken. Patterns of the main inlet reingestion are shown in Figures 26-28.

VII. EXPERIMENTAL RESULTS AND INTERPRETATION

A. POTENTIAL FLOW SOLUTION

The digital potential flow solution yielded a result which indicated that "supercirculation" was present at the rearmost canard flap. Here supercirculation was defined to occur when a streamline circumscribed any particular lifting surface. Supercirculation was present throughout the range of variables of velocity in the diffuser and mass flow distribution entering the canard augmentor. There was also a rapid return of the exhaust profile to freestream conditions only a few chord lengths aft of the canard.

The electrostatic analogy solution eliminated inaccuracies in the coarse mesh size. The flow around the canard was absent of supercirculation. However, a stagnation point was produced on the upper surface of the rear canard flap. The influence of the wing and its exhaust was apparent in its influence on the canard flow. The tendency of the canard exhaust jet to return to freestream conditions was negated by the presence of the wing and its flow field. The highest velocities in the flow field occurred between the wing and the simulated ground. The bending of the exhaust jets and resultant vortex shedding was evident primarily around the wing. Supercirculation was evident around the rearmost flap of the wing for this case.

Using the results of the electrostatic analogy as an indication of the velocity and shape of the exhaust jets,

an analysis was done to determine the effect of the exhaust jets and vortex shedding on the lift of the aircraft. Using the results shown in Figure 4, the radii of curvature of the exhaust streamlines and the distances between the adjacent streamlines in the normal direction were measured graphically. This was done in the vicinity of the trailing edge of the rear wing flap.

The rate of change of pressure in the normal direction is related to the local dynamic pressure and streamline radius of curvature by

$$\rho_a \frac{U^2}{R_{ij}} = - \frac{\partial P}{\partial n} . \qquad (13)$$

Considering streamlines one and two of Figure 4, the above equation can be integrated to yield the following result.

$$P_2 - P_1 = - \rho_a \frac{U^2}{R_{12}} (n_2 - n_1). \qquad (14)$$

Nondimensionalizing the pressure difference with respect to the freestream dynamic pressure, the following relation can be derived.

$$\frac{(P_2 - P_1)}{q_\infty} = - \frac{2(\Delta n_\infty)^2}{R_{12}(n_2 - n_1)} . \qquad (15)$$

The results of these measurements and a resultant pressure coefficient across the exhaust jet are shown in Appendix C.

Further, since the lift coefficient can be represented by the difference in the average pressure at the top of a surface and the bottom of the surface divided by the dynamic pressure, the resultant value for $\Delta P/q_\infty$ across the jet is analogous to a lift coefficient. The numerical value for

the pressure coefficient across the jet is greater than that which would have been obtained from a three-dimensional application of potential flow.

B. RECIRCULATION

Recirculation was most severe in the VTOL configuration when the aircraft was situated on the ground. The main inlet was the largest recipient of exhaust gases. In general, reingestion decreased as height above the ground increased. However, for some cases, reingestion increased as height aobve the ground increased and then decreased again as the height was further increased; for example, see Figure 15, $\theta = 60°$, and Figure 16, $\theta = 90°$. The highest readings resulted when the point of introduction was at the forward Coanda slot of the canard.

The results of introducing freon into the canard or wing were not independent of the point of introduction. Usually there was considerable difference in the response from station to station within the wing or canard. For example, see Figures 14, 15, and 16 for the response of the main inlet to introduction points within the canard.

The angle that the wing and canard made with the ground had considerable influence on recirculation. With the wing and canard at an angle of 60 degrees with the ground, the wing was never a source of reingestion. The canard provided some reingested gases at all altitudes and configurations. Deviations in wing and canard angle with the vertical resulted in a substantial reduction of reingestion for all altitudes and configurations.

The distribution tests at the main inlet indicated that reingestion was concentrated most heavily on the side most distant from the plane of symmetry of the aircraft when the point of introduction was station 1; see Figure 13 for station identification and Figure 26 for the measured result. For station 2, however, the reingestion properties were most pronounced at the upper portion of the main inlet; see Figure 27. When freon was introduced into station 3, there was an even distribution over the entire main inlet face; see Figure 28. The level of reingestion was only trace for this case.

The response time for all reingestion readings was small, indicating that the fountain effect was the only effect contributing to recirculation. There was no opportunity for the "buoyant" effect to be felt, however, since there was no significant temperature difference between the primary and ambient air. Responses occurring a considerable length of time after the introduction of freon were attributed to diffusion and mixing of freon into the ambient air. These responses were never greater in magnitude than trace.

VIII. CONCLUSIONS AND RECOMMENDATIONS

A. CONCLUSIONS

The potential flow solution was valuable in obtaining an approximation to the pressure coefficient across the exhaust jet. This coefficient provided insight into the contribution of a two-dimensional propulsive lift jet to the flow field of the aircraft.

Reingestion poses a problem primarily to the main inlet under VTOL conditions. The magnitude of the problem was greater than the 18% obtained with moderate reingestion for all altitudes. The canard was the most significant source of reingested exhaust gases, and was the only source to supply readings above moderate. The wing contributed no gases for reingestion in configurations other than VTOL.

B. RECOMMENDATIONS

Further work would be desirable to determine the effect of a forward velocity as simulated in the wind tunnel on reingestion properties. Closer scrutiny might be applied to the flow path from the canard ejector and Coanda slots to the main inlet.

APPENDIX A: SAMPLE DERIVATION OF DIFFERENCE EQUATION

Each linear, algebraic equation was derived as follows

$$\begin{array}{ccc} & \psi(x,y+k) & \\ & \vdots\ j & \\ \psi(x-j,y) \cdots & & \cdots \psi(x+j,y) \\ & k & \\ & \psi(x,y-k) & \end{array}$$

beginning with Taylor series for each axis of the domain.

$$\psi(x,y+k) = \psi(x,y) + \frac{k\partial\psi}{\partial y}(x,y) + \frac{k^2}{2!}\frac{\partial^2\psi}{\partial y^2}(x,y) + \ldots$$

and

$$\psi(x,y-k) = \psi(x,y) - \frac{k\partial\psi}{\partial y}(x,y) + \frac{k^2}{2!}\frac{\partial^2\psi}{\partial y^2}(x,y) - \ldots$$

Adding the above equations and solving for the second partial, the following equation results.

$$\frac{\partial^2\psi}{\partial y^2} = \frac{2}{k^2}\left[\ \psi(x,y+k) - 2\psi(x,y) + \psi(x,y-k)\ \right] + 0(4).$$

Similar analysis for the second partial in the x-direction yields

$$\frac{\partial^2\psi}{\partial x^2} = \frac{2}{j^2}\left[\ \psi(x+j,y) - 2\psi(x,y) + \psi(x-j,y)\ \right] + 0(4).$$

Applying Laplace's equation

$$\frac{\partial^2\psi}{\partial x^2} + \frac{\partial^2\psi}{\partial y^2} = 0$$

each solution point is represented as a linear function of its four adjacent points.

$$\psi(x,y) = \frac{j^2}{2(j^2+k^2)}\left[\ \psi(x,y+k) + \psi(x,y-k)\right] + \frac{k^2}{2(j^2+k^2)}$$
$$\left[\ \psi(x+j,y) + \psi(x-j,y)\right].$$

APPENDIX B: MASS FLOW RATE CALCULATIONS OF QUANTITATIVE ANALYSIS

The following data was obtained either experimentally or from tables of known properties of freon or air.

$\rho_a = 7.66 \times 10^{-2}$ lbm/ft^3

$\rho_f = 2.028$ lbm/ft^3

$U_1 = 567$ ft/sec

$U_2 = 136$ ft/sec

$U_p = 0.45$ ft/sec

$U_4 = 27.5$ ft/sec

$A_1 = 4.91 \times 10^{-4}$ in^2

$A_2 = 0.807$ in^2

$A_p = .0204$ in^2

$A_4 = 4.3$ in^2

The mass flow rates used in the quantitative analysis were calculated using the above data and appropriate conversion factors to maintain consistency in units.

$\dot{m}_1 = \rho_f U_1 A_1 = 3.92 \times 10^{-3}$ lbm/sec

$\dot{m}_2 - \rho_a U_2 A_2 = 4.58 \times 10^{-1}$ lbm/sec

$\dot{m}_3 = \rho_a U_p A_p = 4.82 \times 10^{-6}$ lbm/sec

$\dot{m}_4 = \rho_a U_4 A_4 = 6.29 \times 10^{-2}$ lbm/sec

APPENDIX C: RESULTS OF POTENTIAL FLOW LIFT JET ANALYSIS

Streamtube i,j	Δn_∞^2	$n_j - n_i$	R_{ij}	$-\frac{2(\Delta n_\infty^2)}{R_{ij}(n_j - n_i)}$
1,2	.39	.25	.75	- 4.16
2,3	.19	.125	1.20	- 2.53
3,4	.19	.156	1.69	- 1.44
4,5	.19	.31	2.38	- 0.53

$$C_L = - \sum - \frac{2(\Delta n_\infty^2)}{R_{ij}(n_j - n_i)} = 8.66$$

Note: Velocity of flow at augmentor exit planes was twice that of freestream conditions.

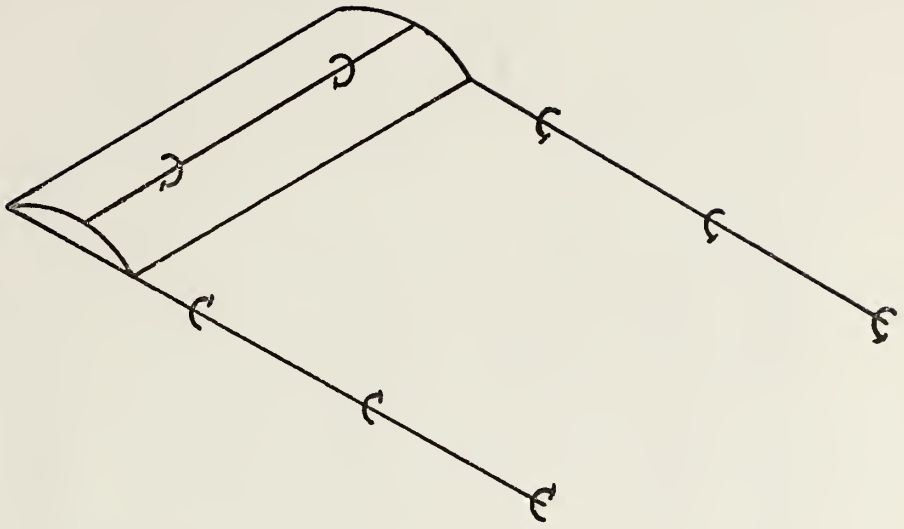

(a) ORDINARY FINITE SPAN WING

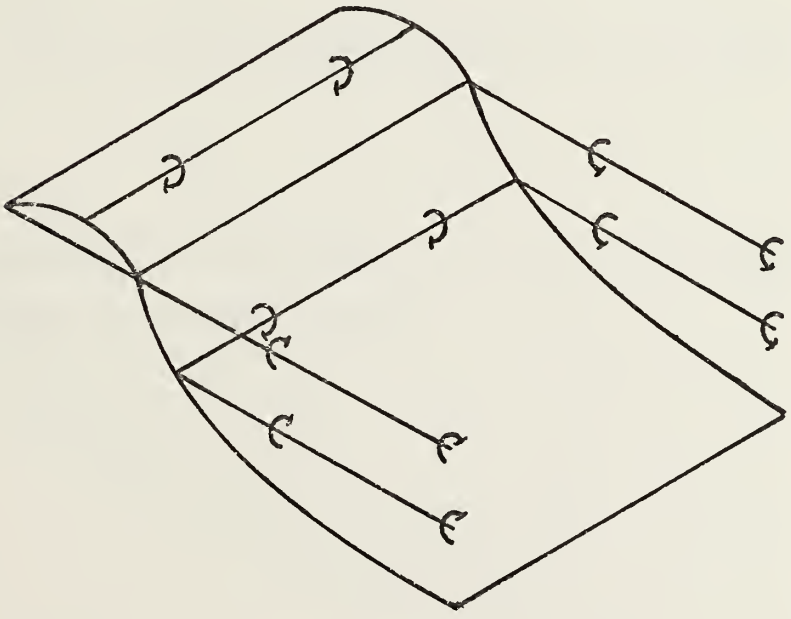

(b) JET FLAP FINITE SPAN WING

Figure 1. SHED VORTICITY ASSOCIATED WITH LIFTING WINGS

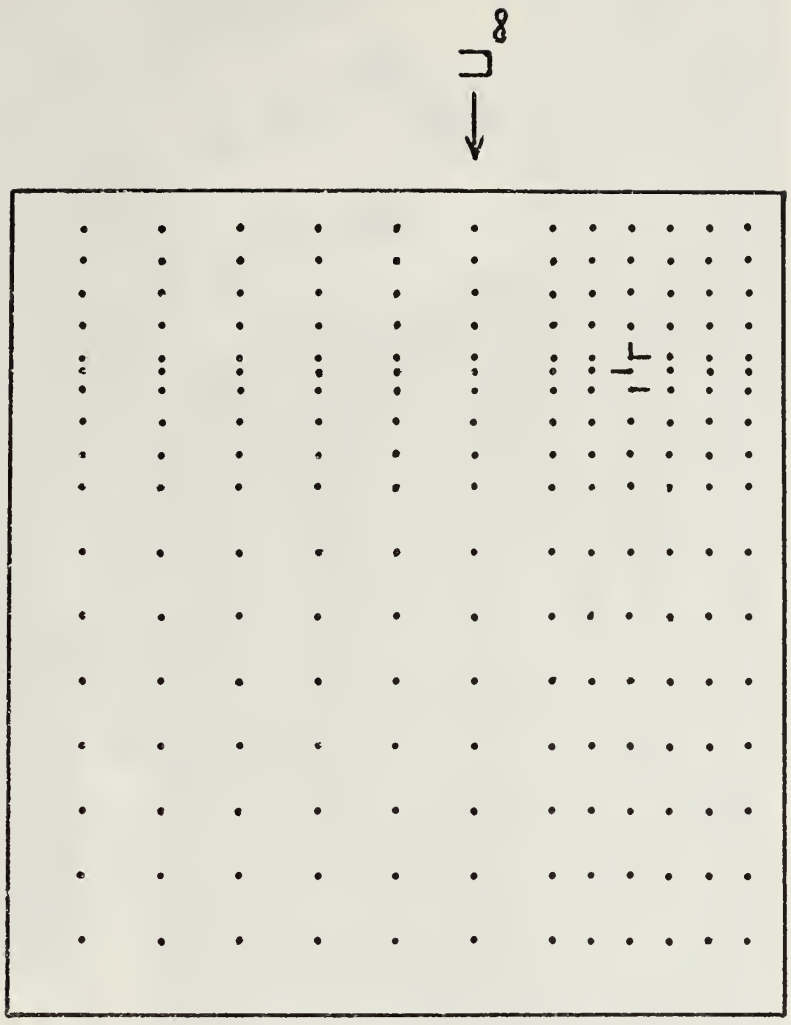

Note: Resultant stream function values are shown in sample computer program output.

Figure 2. DISCRETIZED DOMAIN.

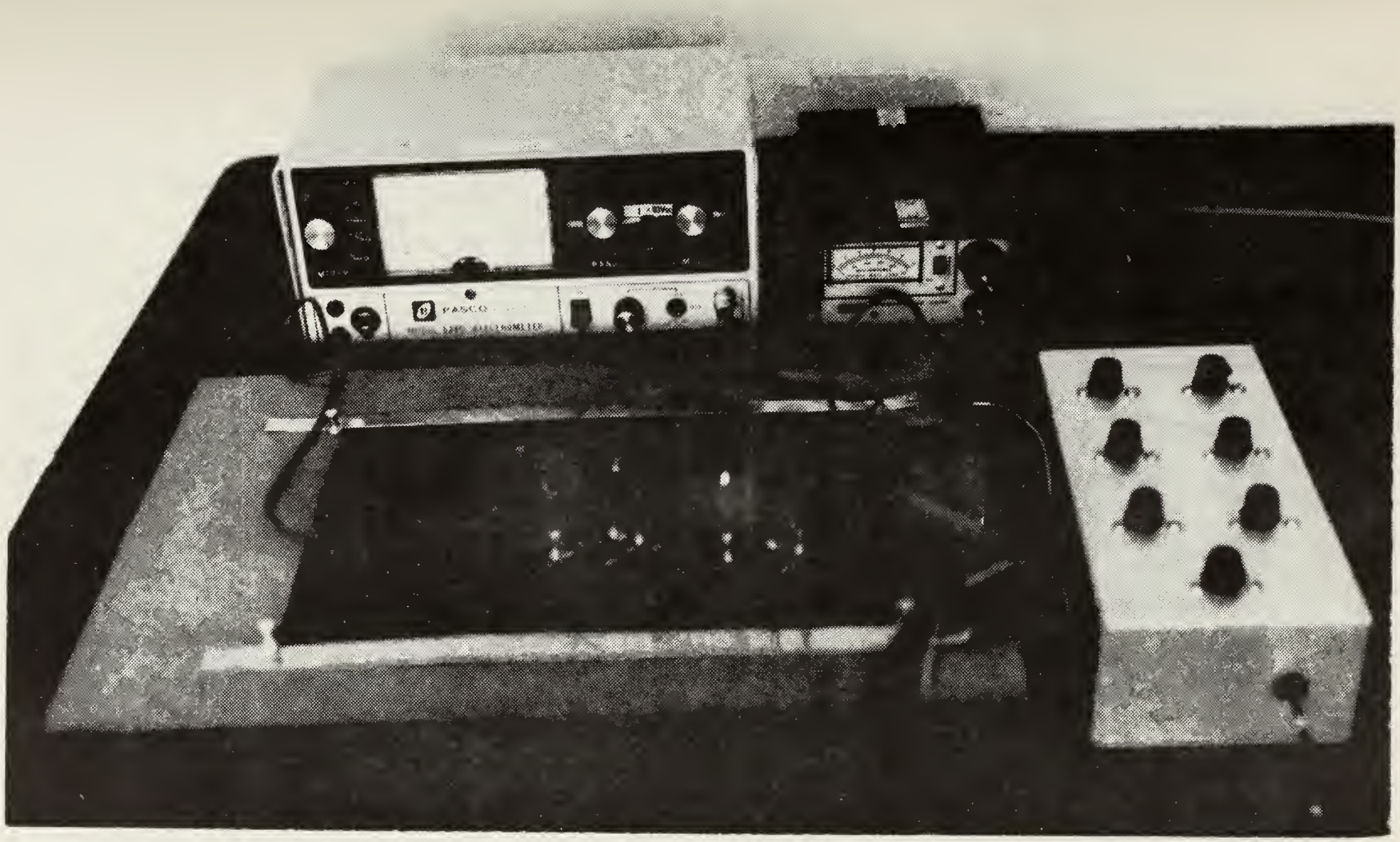

Figure 3. ELECTROSTATIC ANALOGY EQUIPMENT.

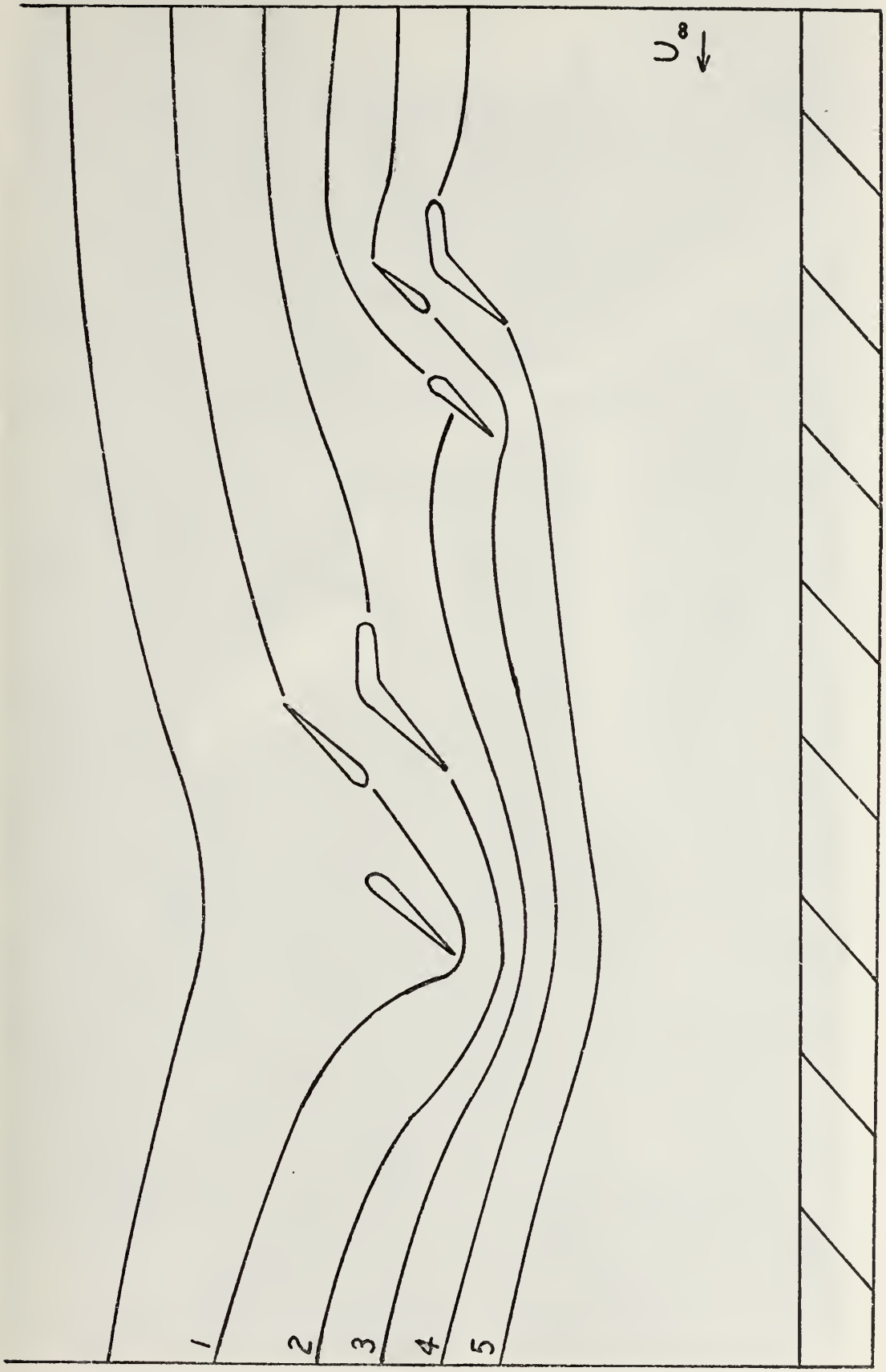

Figure 4. ELECTROSTATIC ANALOGY RESULTS.

Figure 5. MODEL SUPPORT, PLENUM, AND HEATER HOSES.

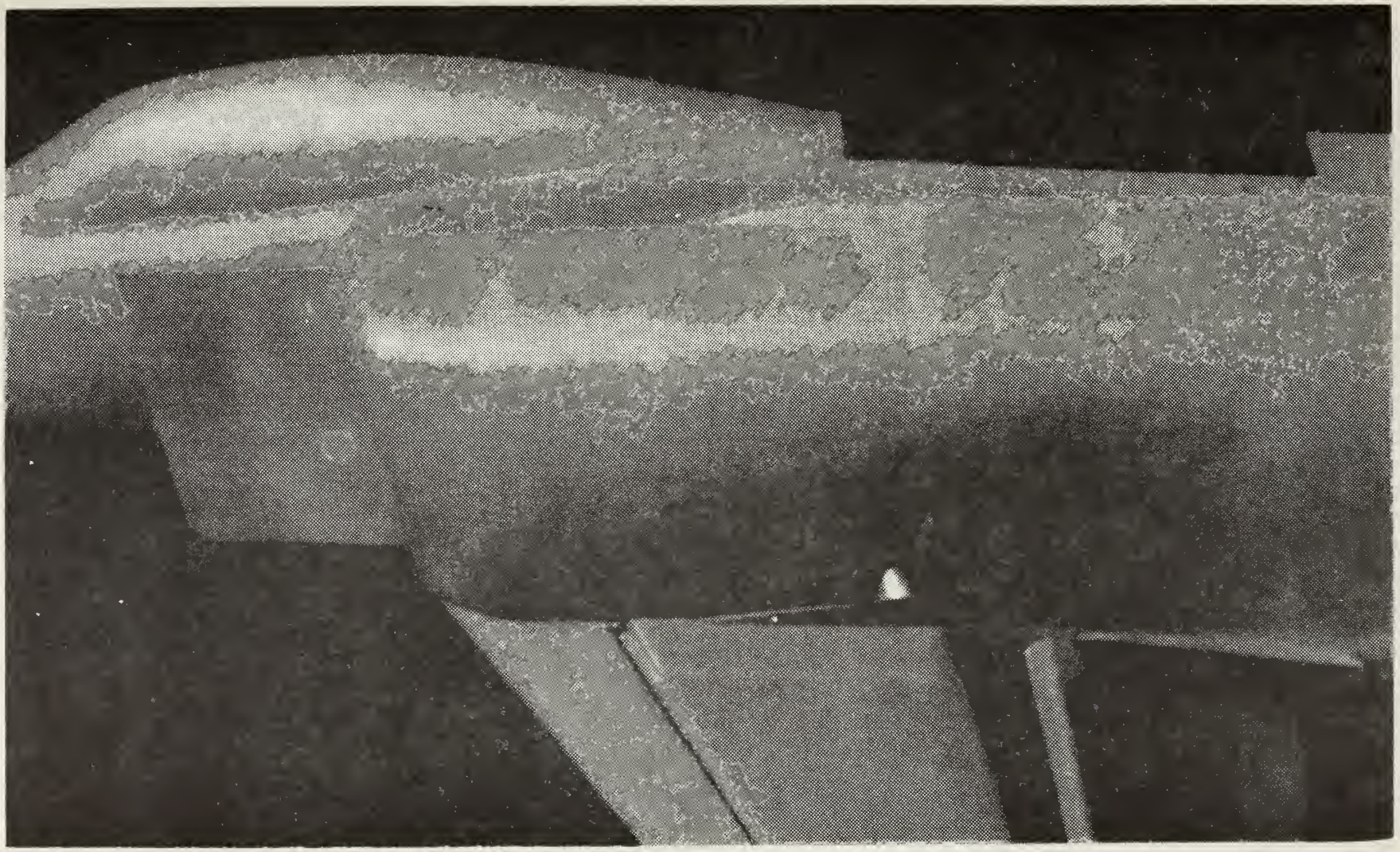

Figure 6. AUXILIARY INLET.

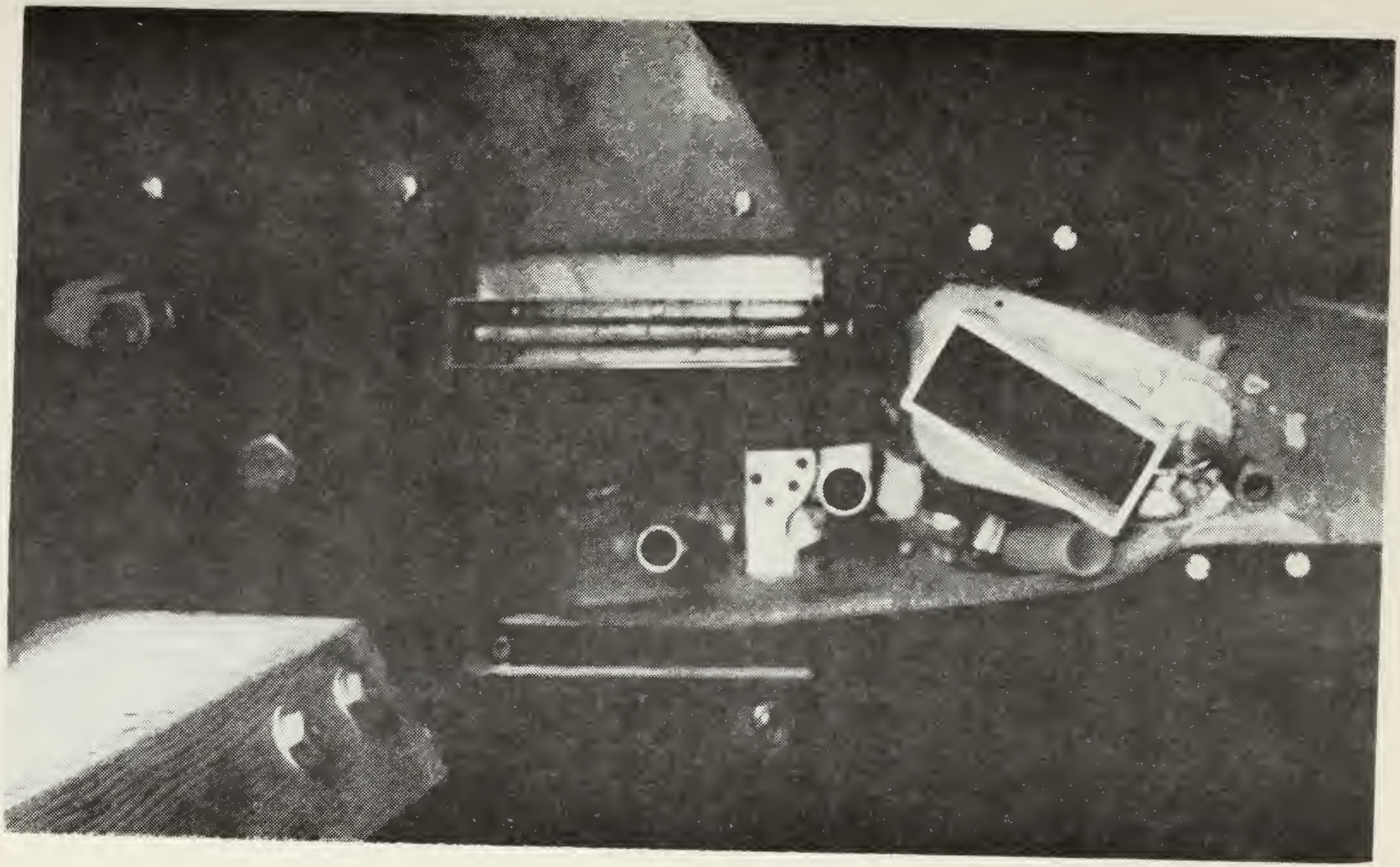

Figure 7. REAR VIEW OF MAIN AND AUXILIARY INLET DUCTS.

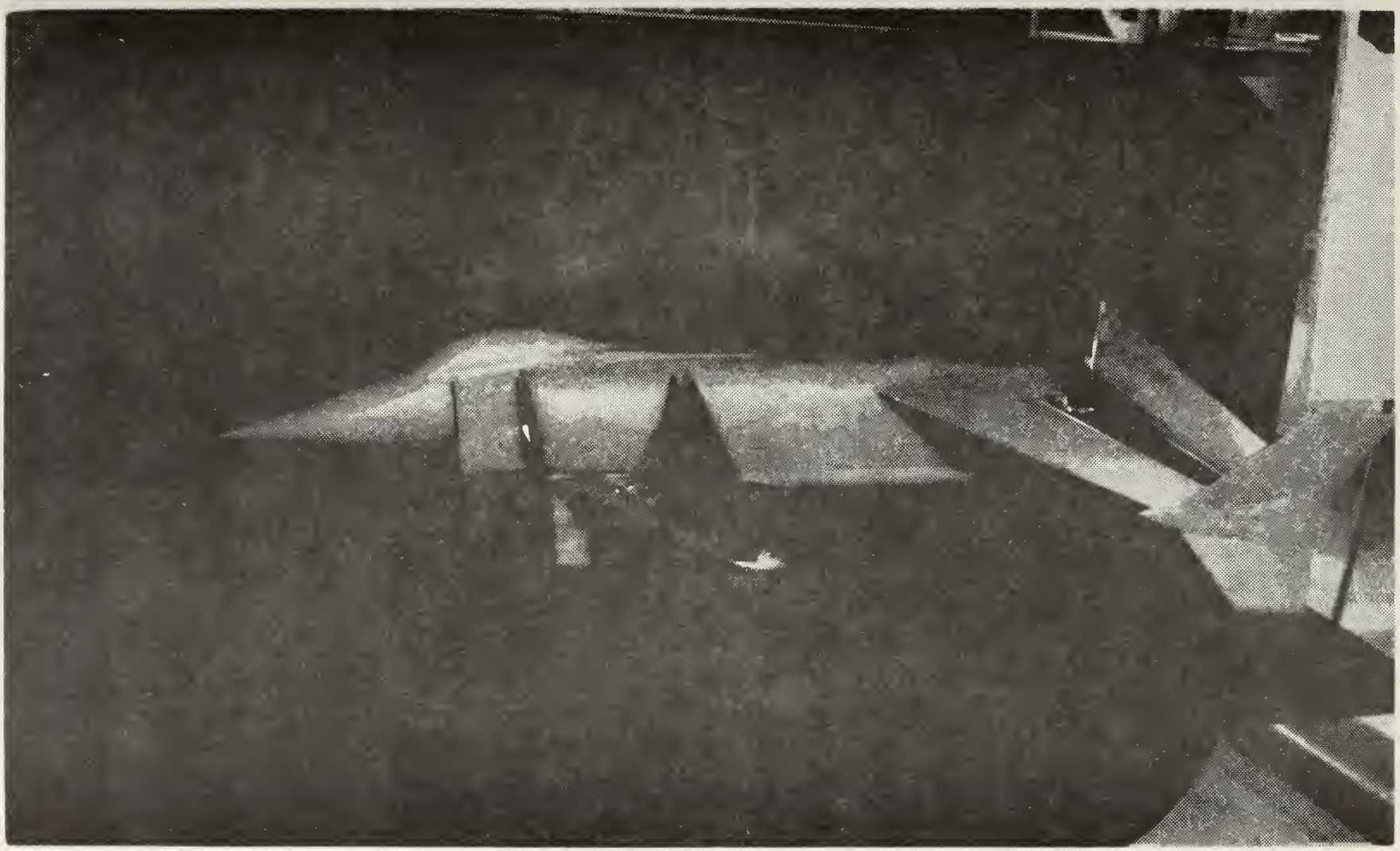

Figure 8. MODEL MOUNTED IN VTOL POSITION AT GROUND HEIGHT.

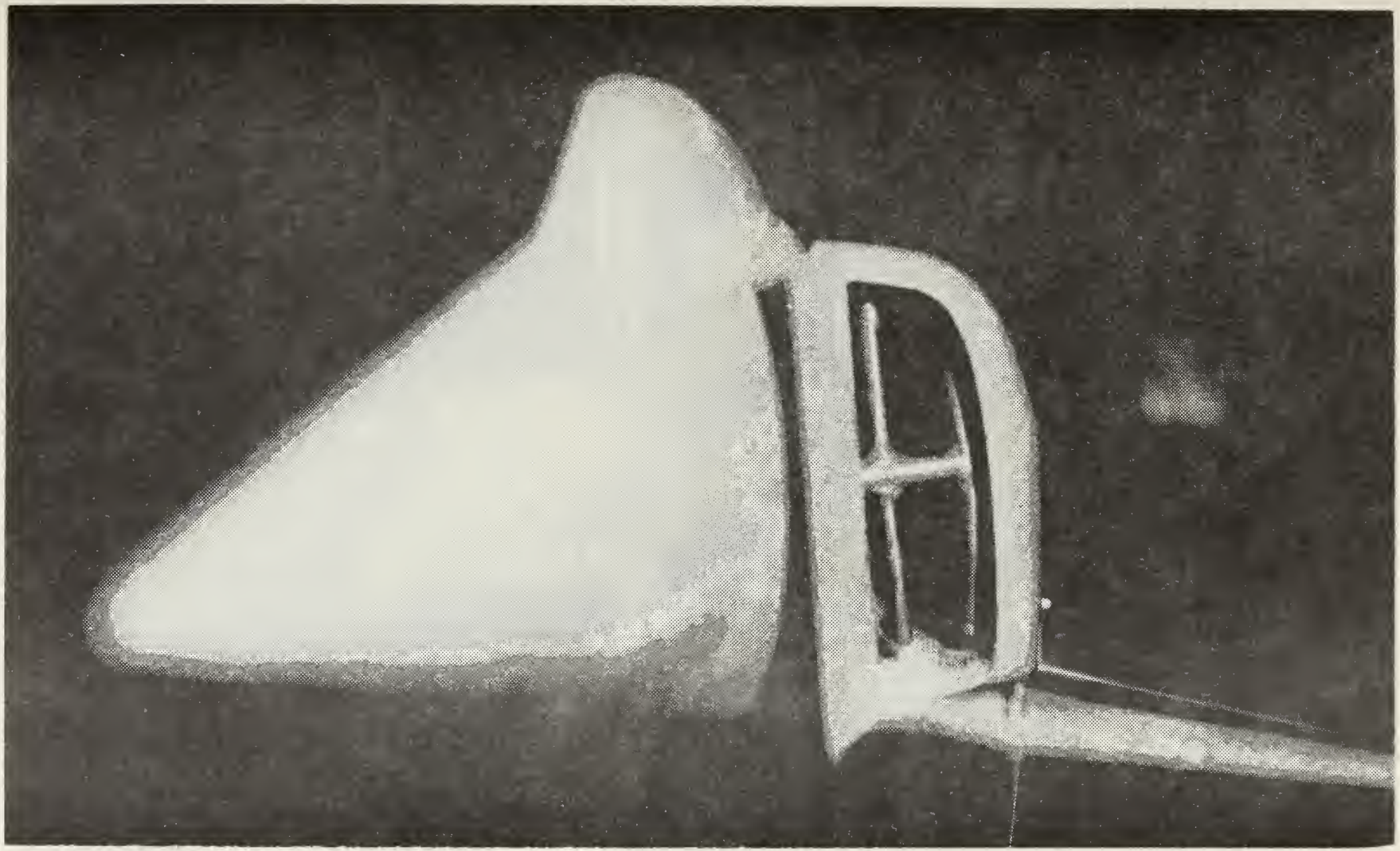

Figure 9. MAIN INLET EJECTOR.

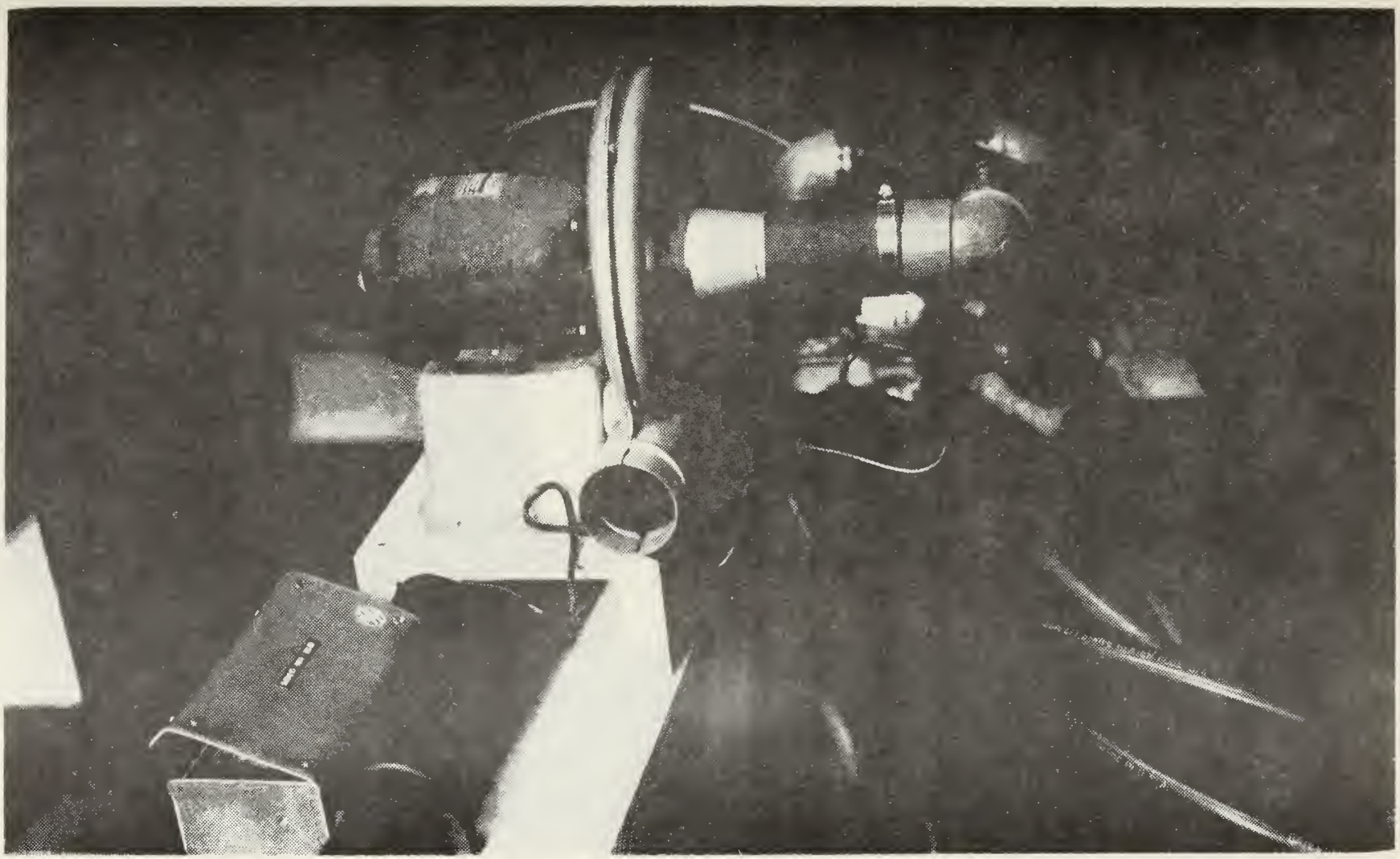

Figure 10. BLOWER WITH ACCOMPANYING DUCTS AND DETECTOR PROBE IN PLACE.

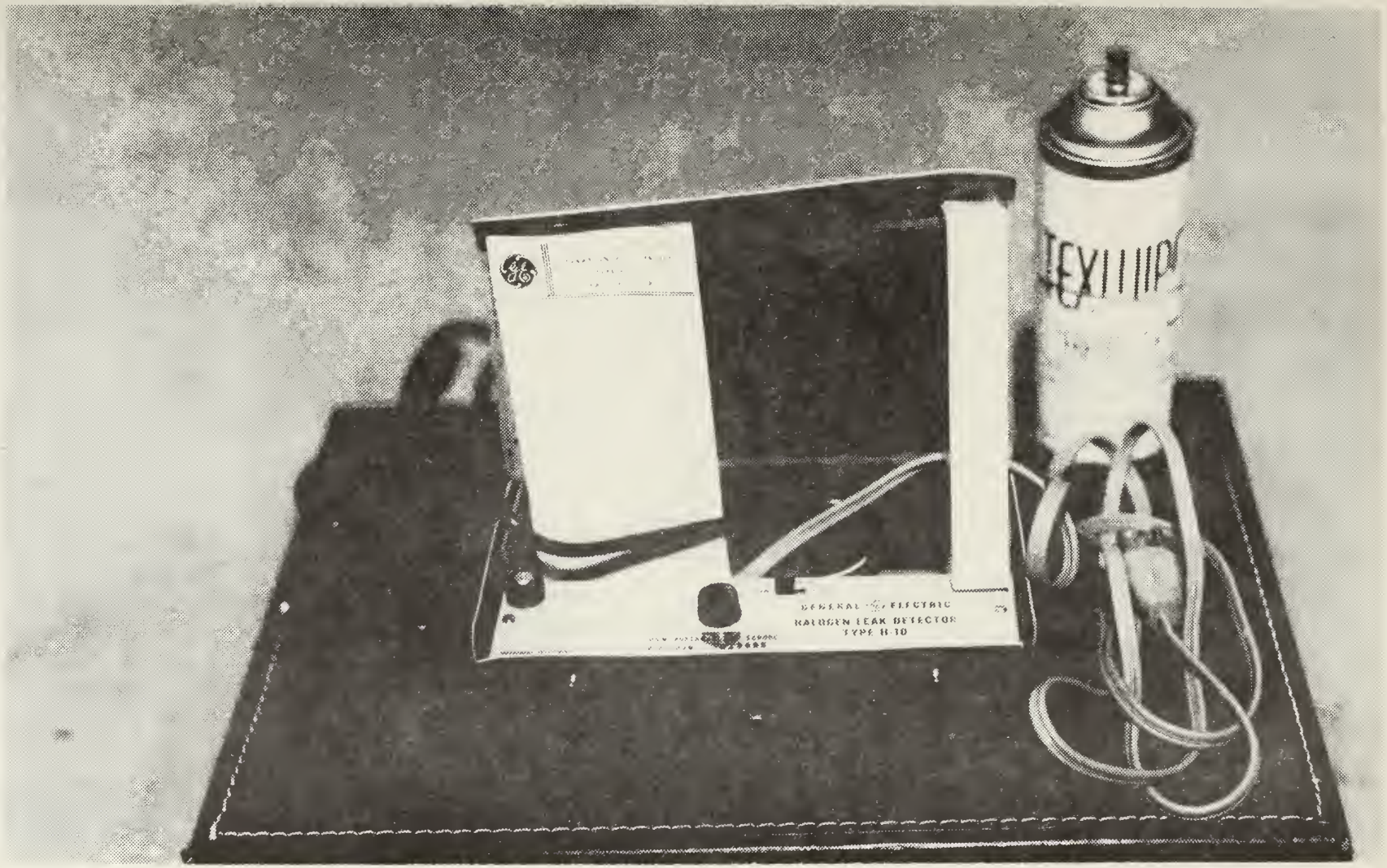

Figure 11. LEAK DETECTOR, PROBE, AND FREON SOURCE.

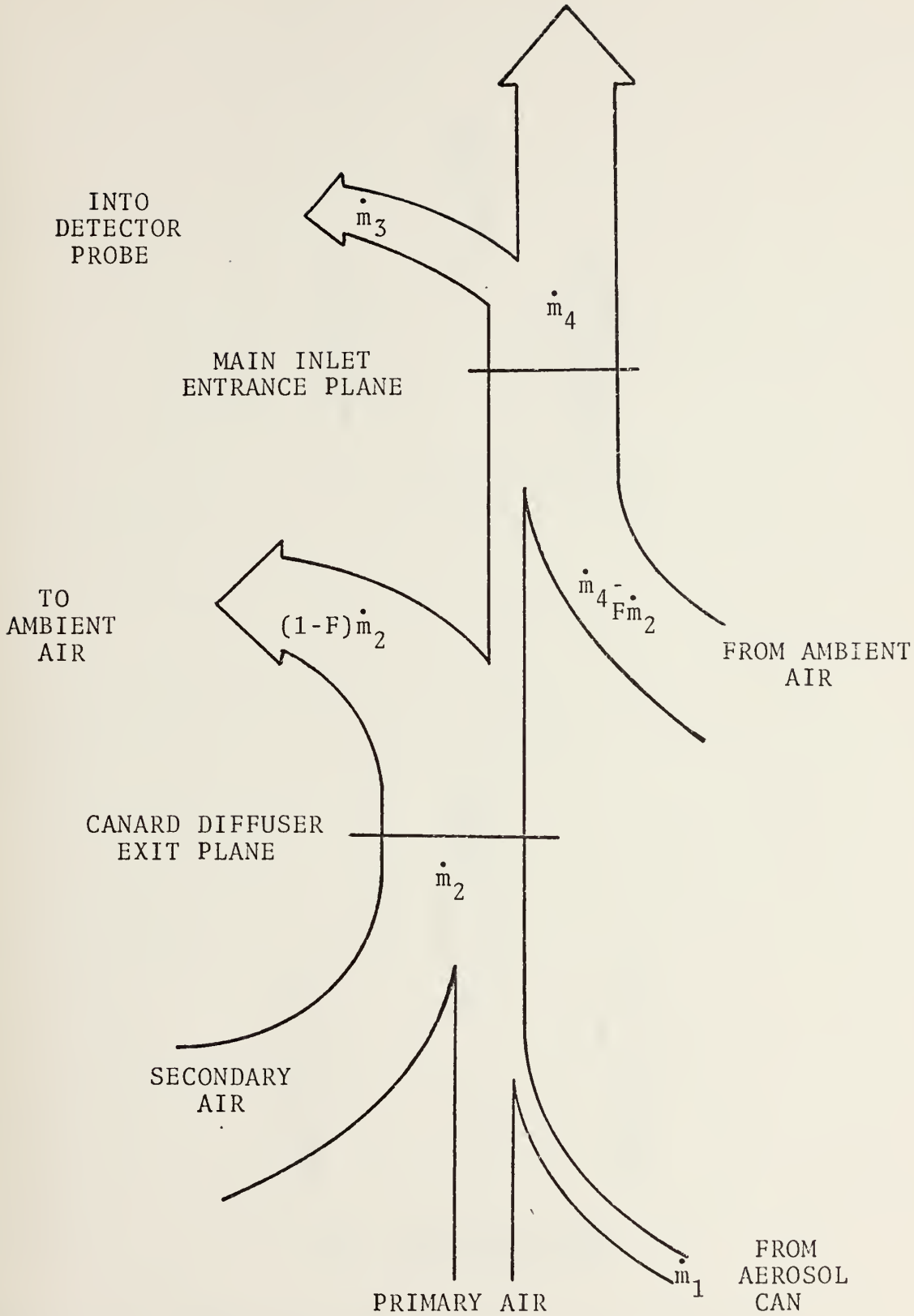

Figure 12. PATH OF REINGESTED EXHAUST GASES.

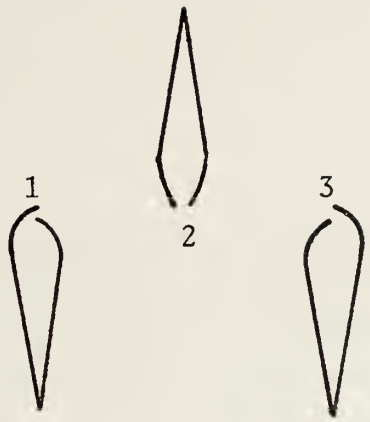

(a) CANARD STATIONS

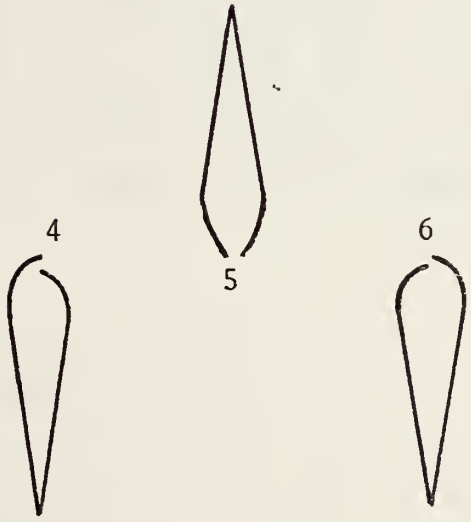

(b) WING STATIONS

Figure 13. IDENTIFICATION OF WING AND CANARD FLAPS.

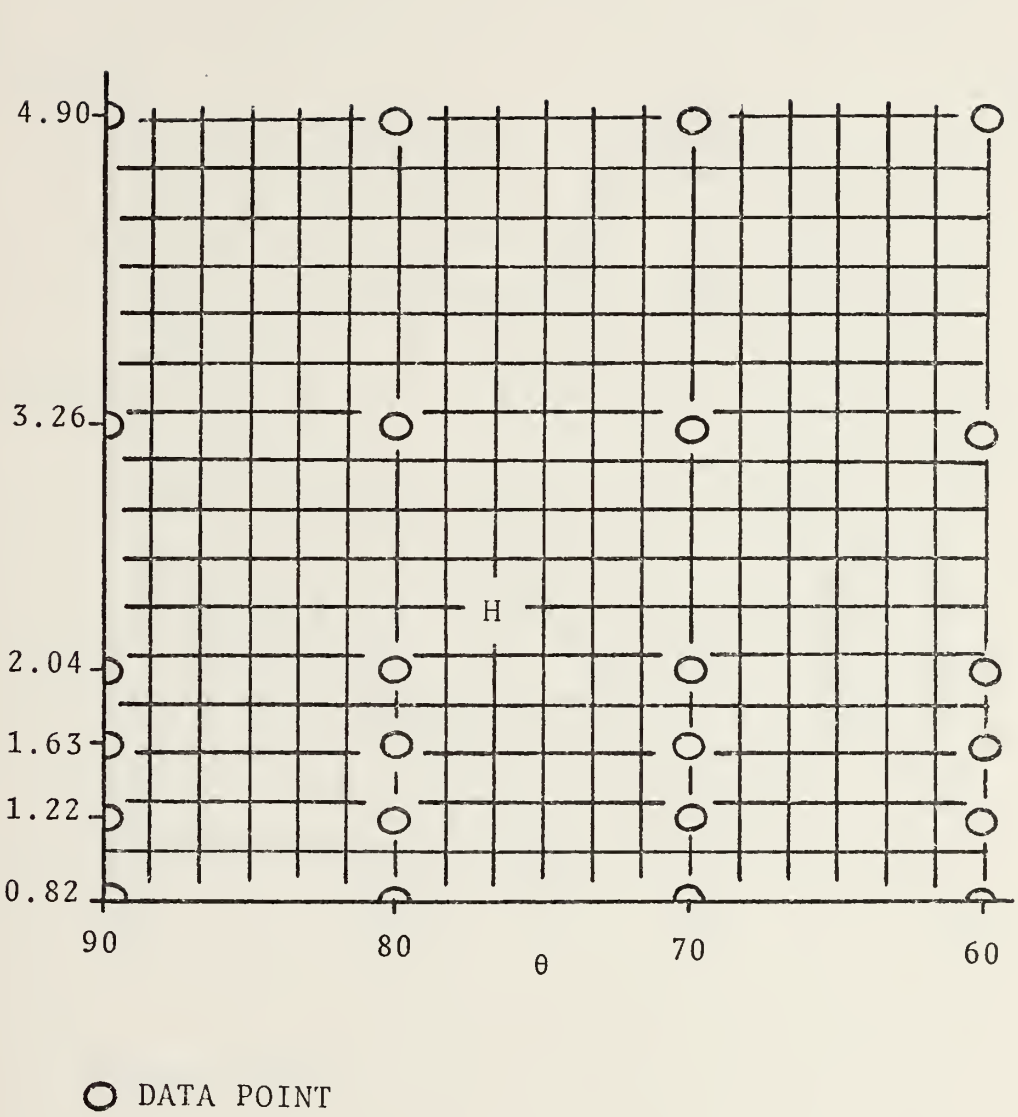

Figure 14. REINGESTION PATTERN; MAIN INLET, STATION 1.

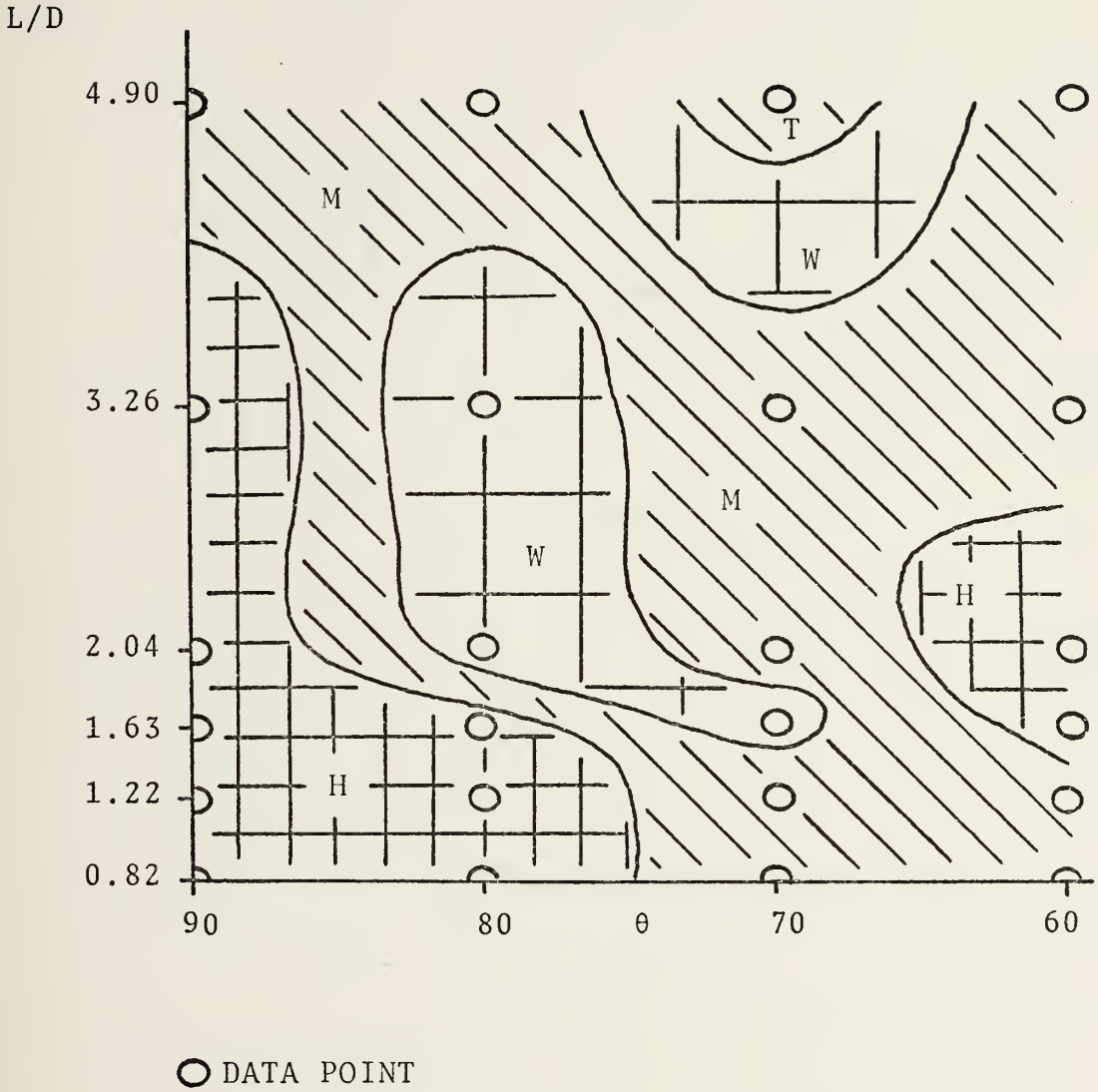

Figure 15. REINGESTION PATTERN; MAIN INLET, STATION 2.

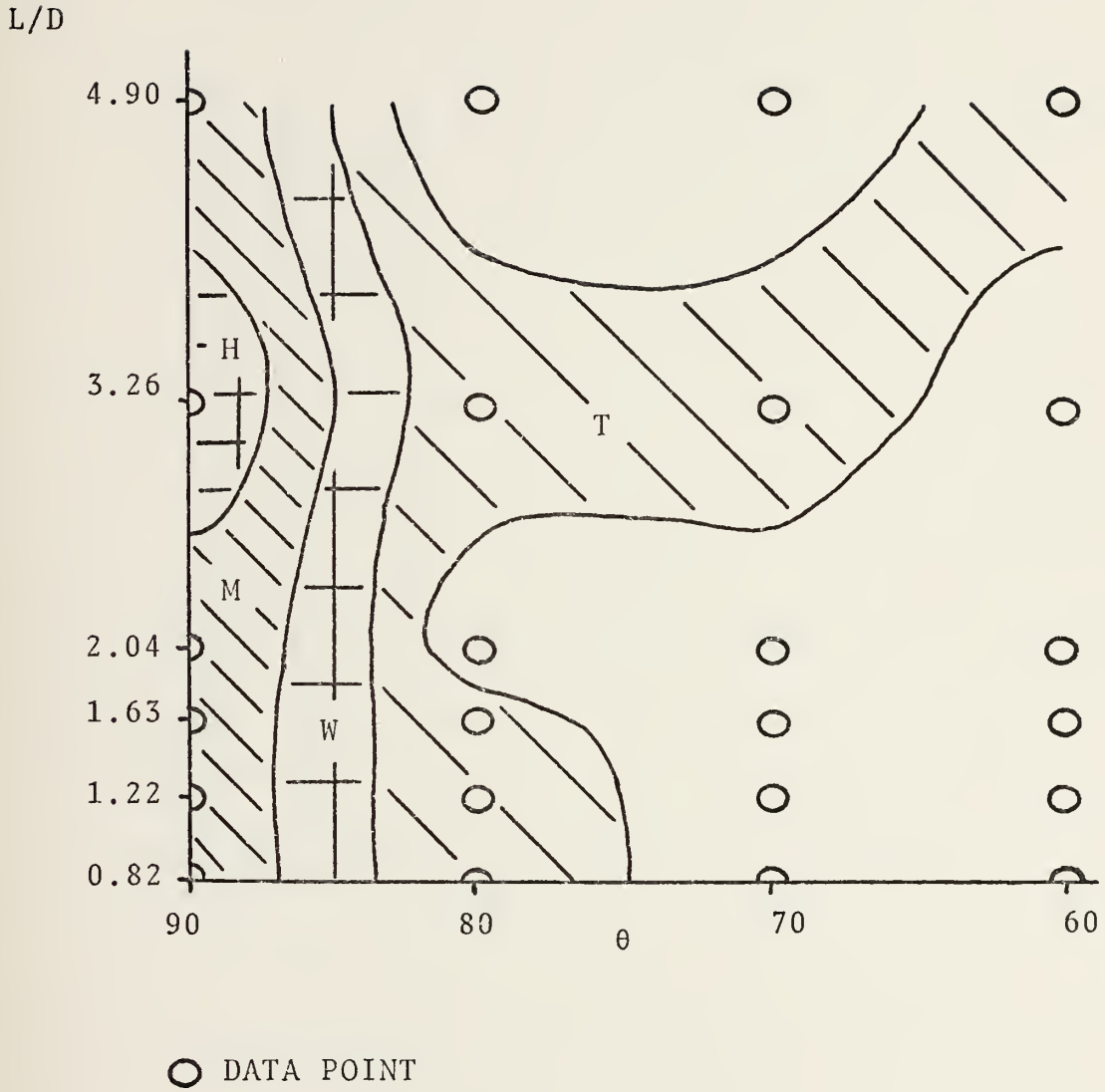

Figure 16. REINGESTION PATTERN; MAIN INLET, STATION 3.

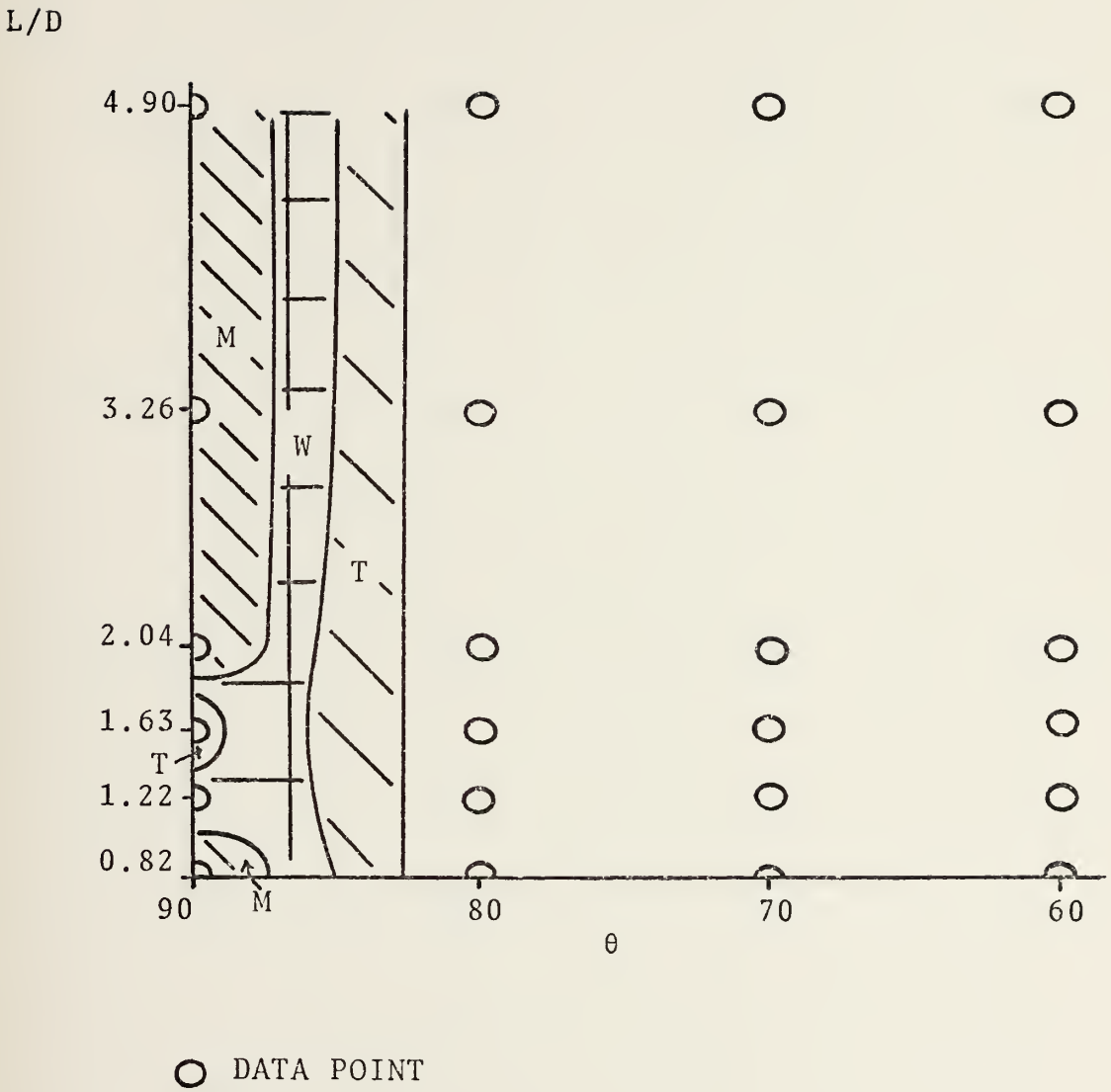

Figure 17. REINGESTION PATTERN; MAIN INLET, STATION 4.

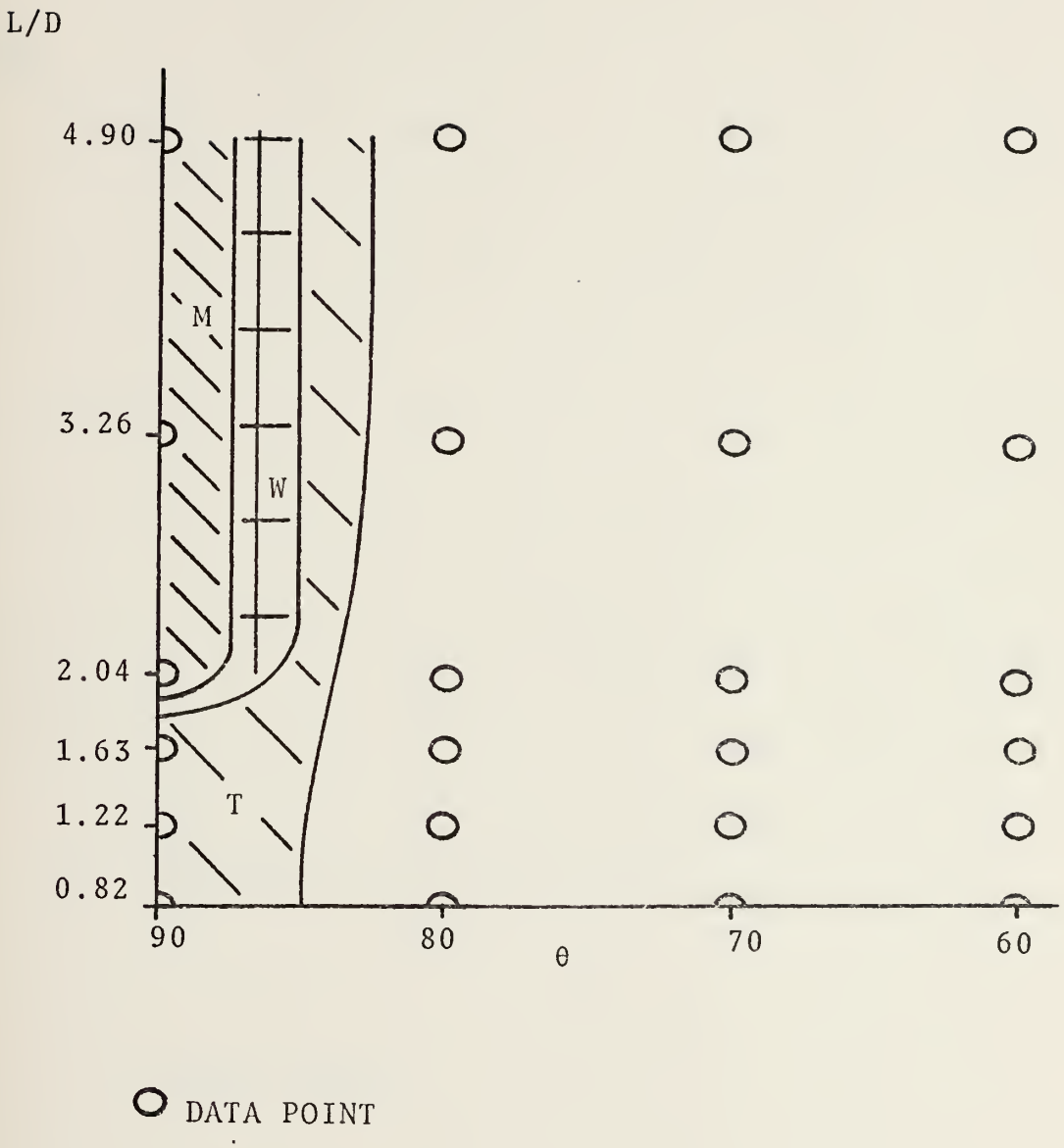

Figure 18. REINGESTION PATTERN; MAIN INLET, STATION 5.

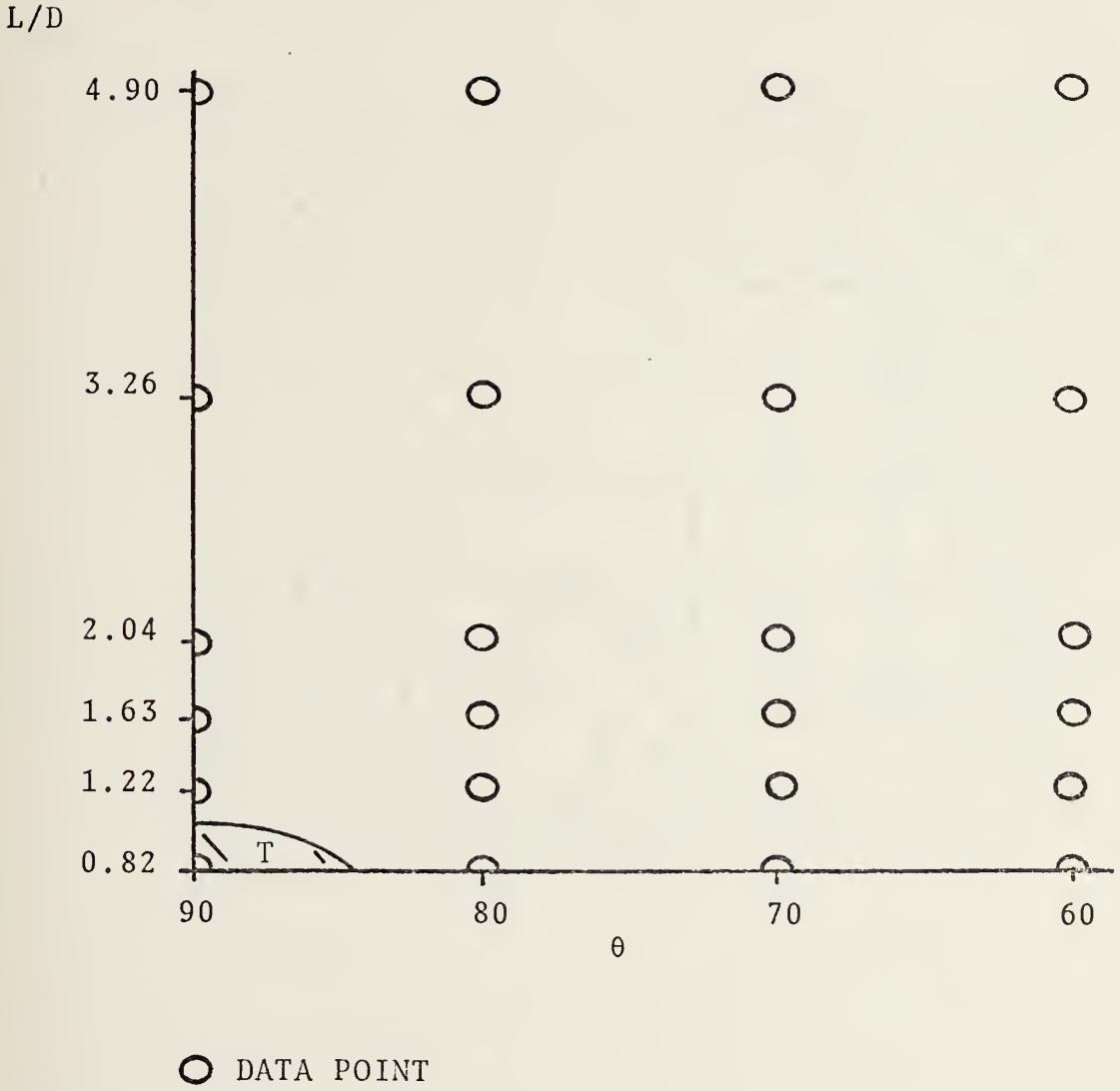

Figure 19. REINGESTION PATTERN; MAIN INLET, STATION 6.

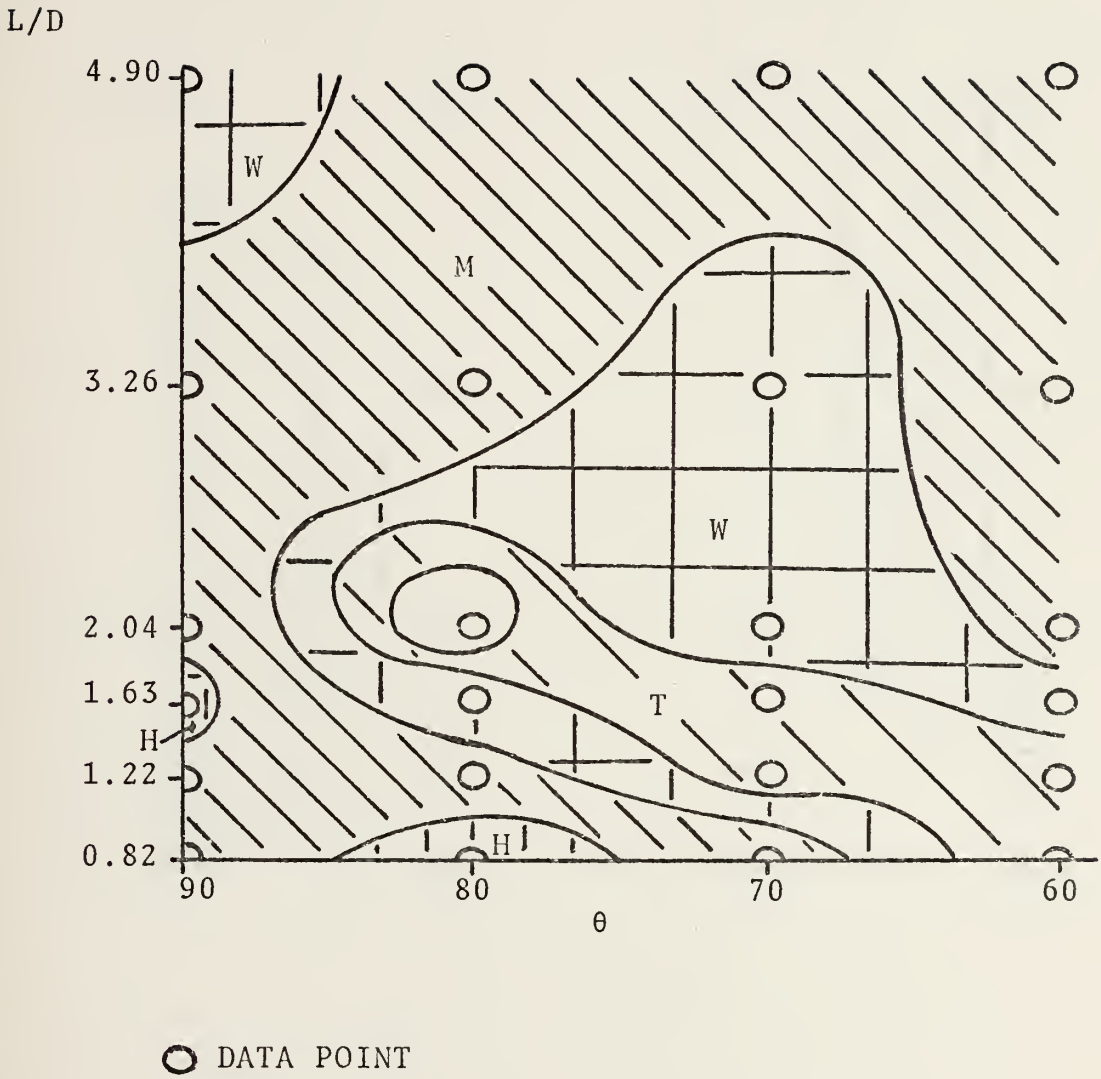

Figure 20. REINGESTION PATTERN; AUXILIARY INLET, STATION 1.

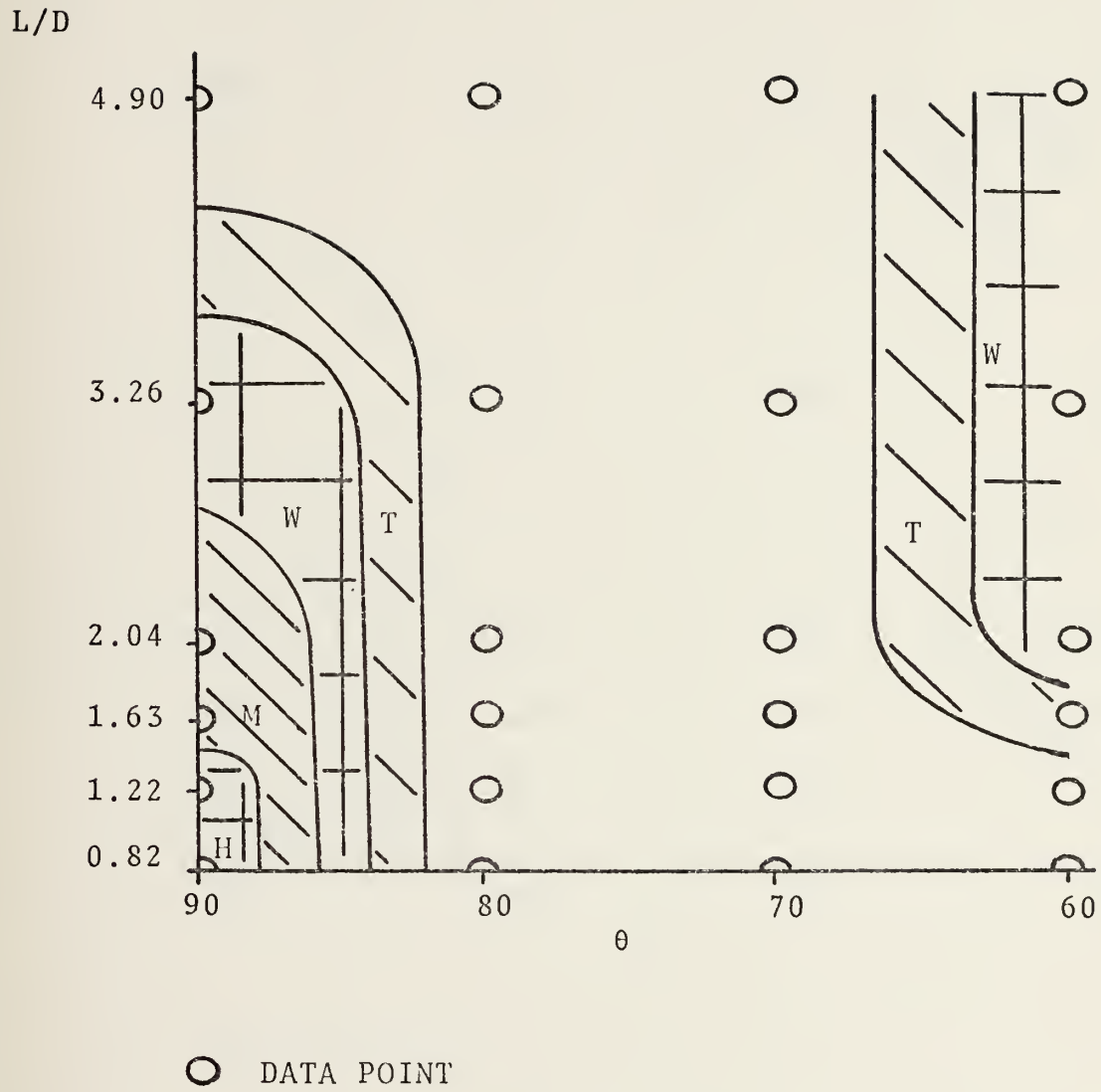

Figure 21. REINGESTION PATTERN; AUXILIARY INLET, STATION 2.

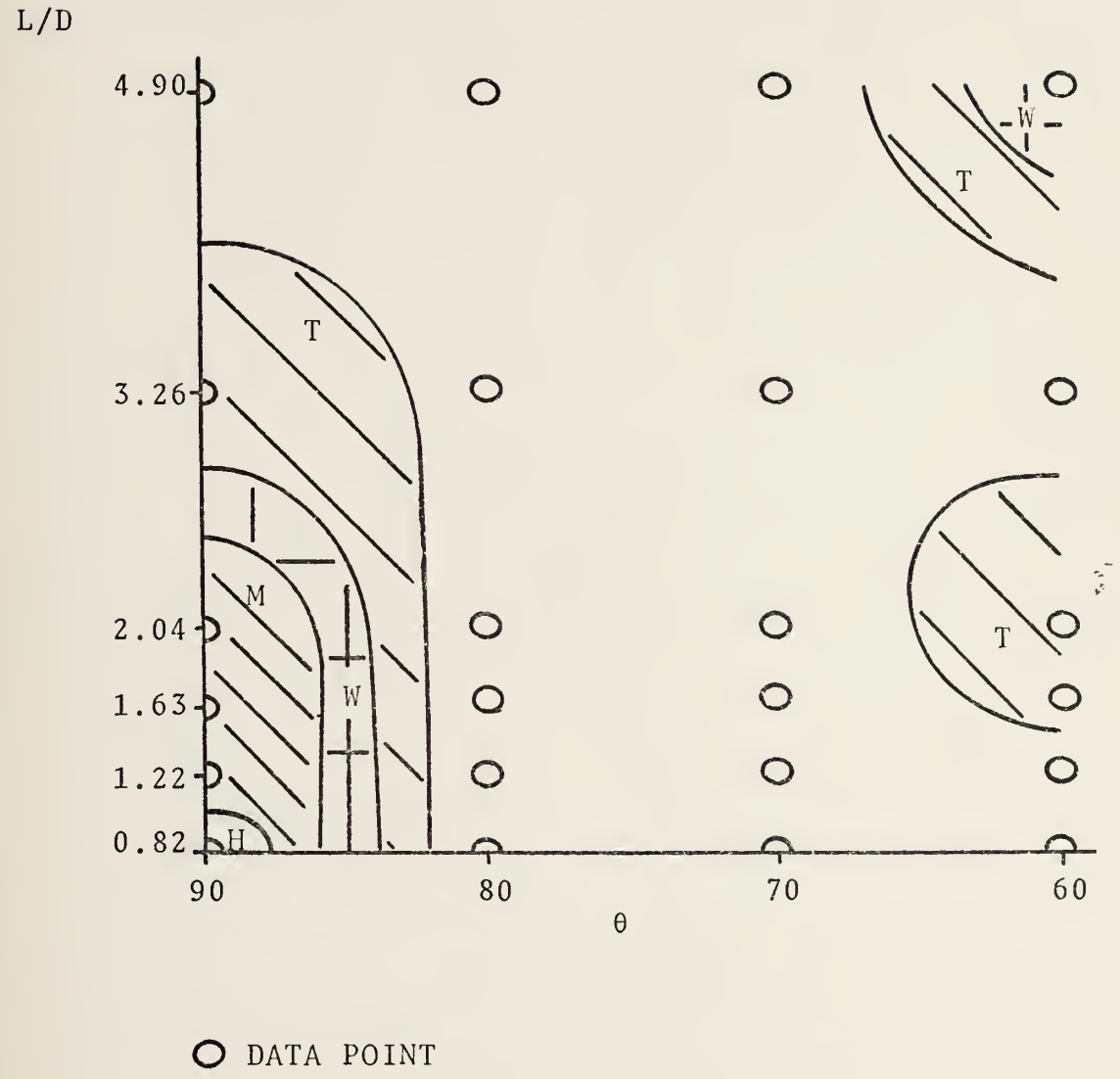

Figure 22. REINGESTION PATTERN; AUXILIARY INLET, STATION 3.

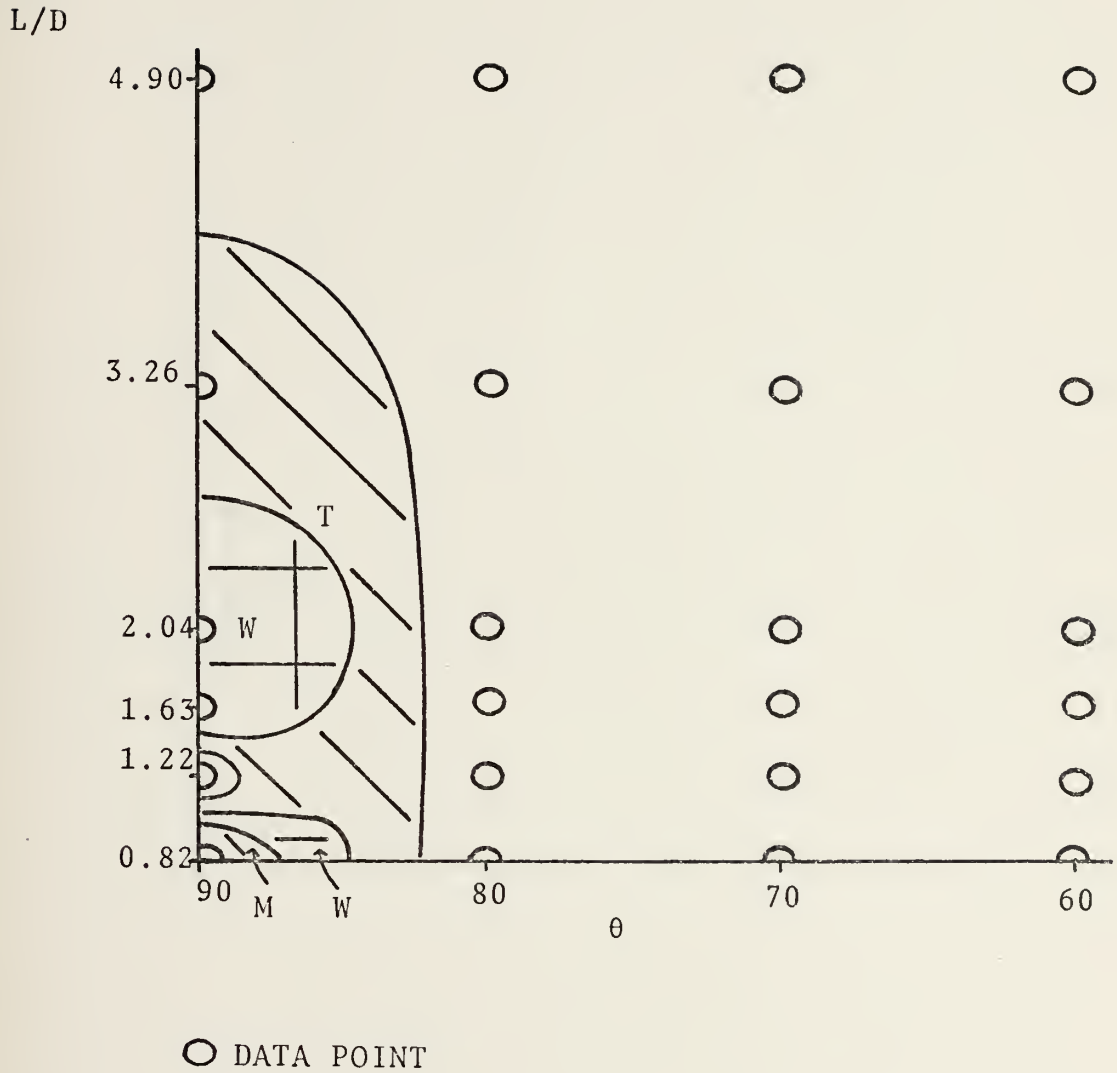

Figure 23. REINGESTION PATTERN; AUXILIARY INLET, STATION 4.

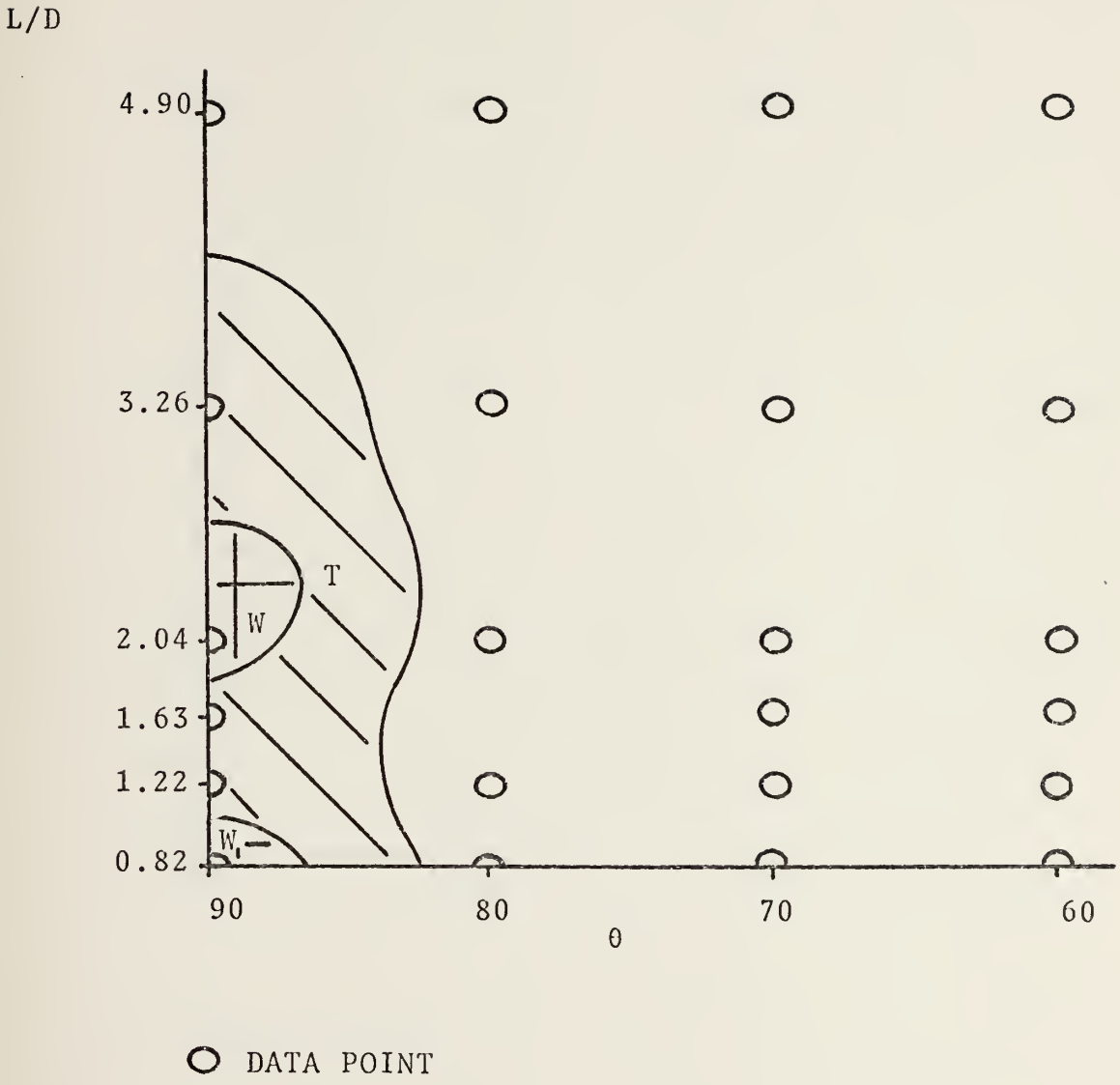

Figure 24. REINGESTION PATTERN; AUXILIARY INLET, STATION 5.

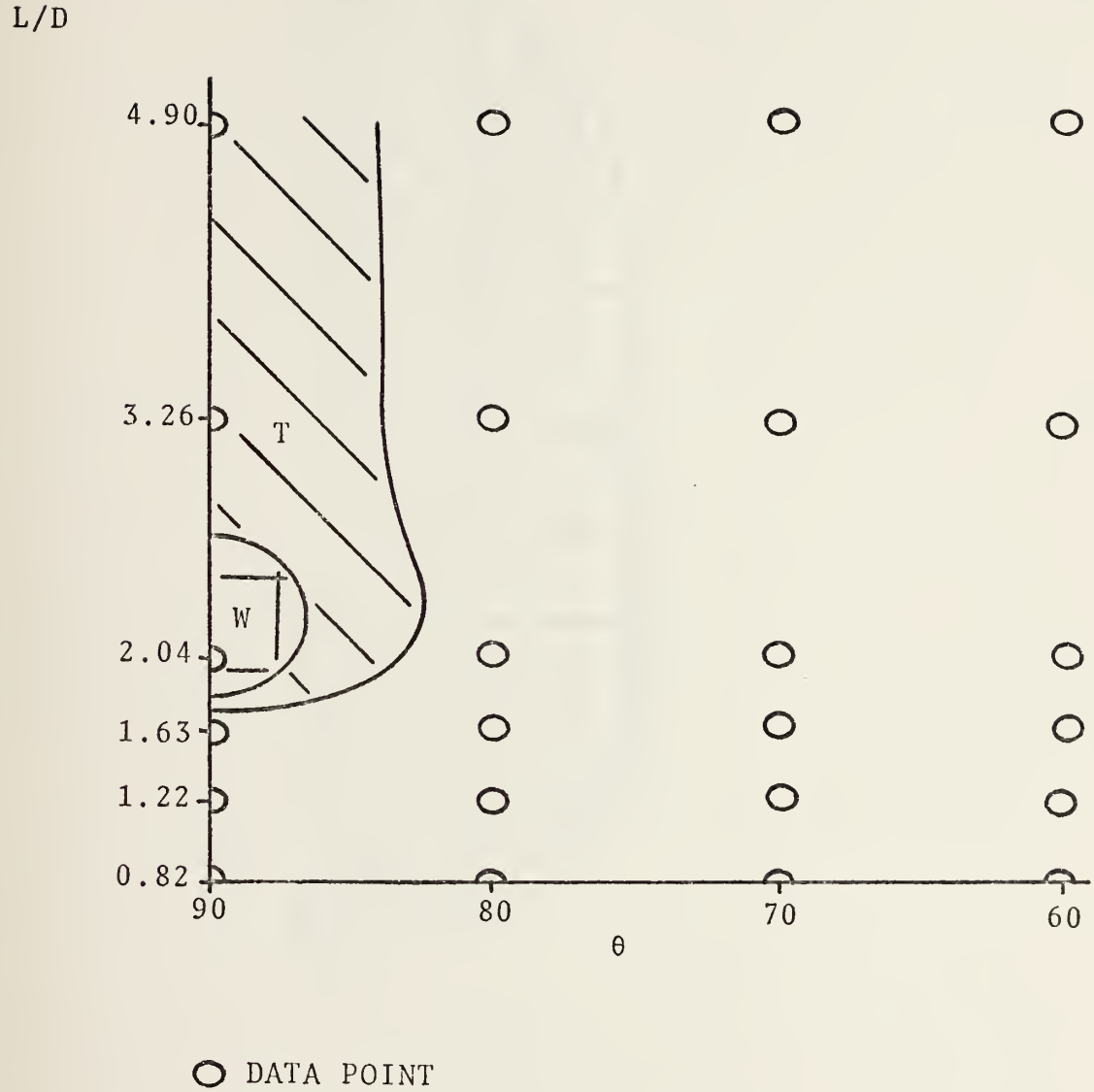

Figure 25. REINGESTION PATTERN; AUXILIARY INLET, STATION 6.

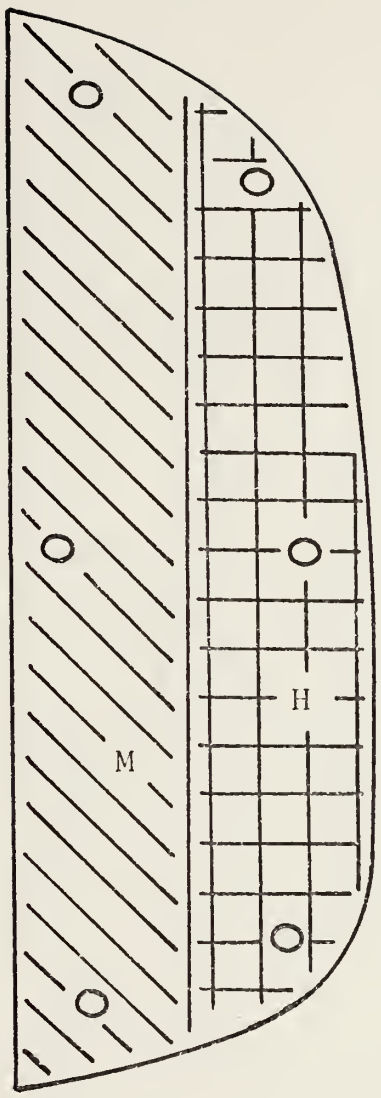

O SAMPLE PORT

Figure 26. REINGESTION PATTERN; MAIN INLET FACE, STATION 1.

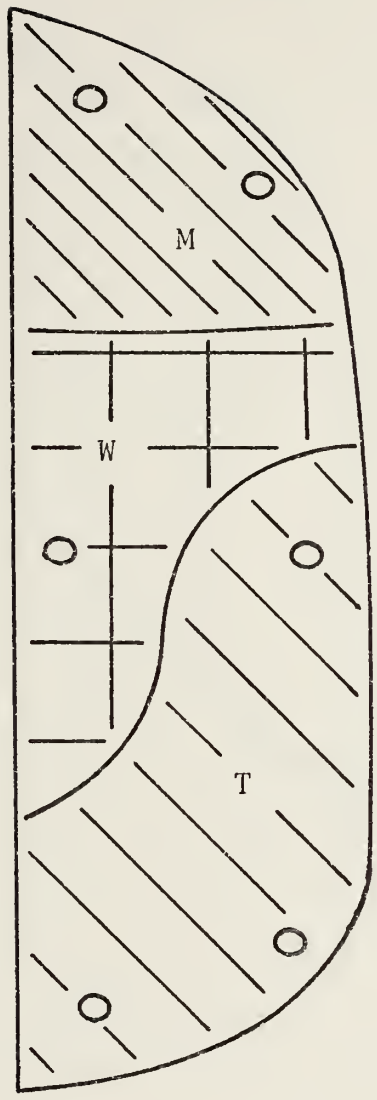

○ SAMPLE PORT

Figure 27. REINGESTION PATTERN; MAIN INLET FACE, STATION 2.

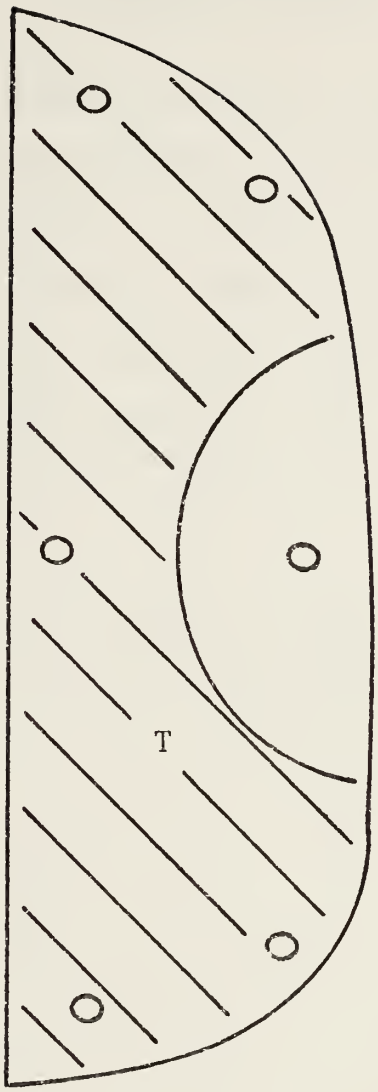

SAMPLE PORT

Figure 28. REINGESTION PATTERN; MAIN INLET FACE, STATION 3.

COMPUTER PROGRAM

On the next page, the text of the computer program begins which solved Laplace's equation using finite difference approximations. A total of nine different runs were made, each of which applied a different combination of velocity at the canard exit plane and ratio of mass flow on each side of the canard ejector. Each combination was obtained by altering the boundary values assigned to the canard flaps.

The results of each of the runs were similar in shape. Consequently, only one of the outputs is included subsequent to the program.

```
  300 FORMAT (//)
  400 FORMAT (6F8.2,6F4.2,//)
  500 FORMAT (6F8.2,2F4.2,4X,3F4.2,//)
  900 FORMAT (//////)
      DIMENSION A(4947),B(201,1),C(201)
      DIMENSION D(201)
C
CC    INPUT THE ELEMENTS OF THE COEFFICIENT MATRIX
C
      DO 5 I = 1,4869
      A(I) = 0.0
    5 CONTINUE
      DO 10 I = 1,201
      C(I) = 0.
   10 CONTINUE
      M = 2
      N = 0
      DO 15 I = 13,69,14
      M = M + N
      J = I + M
      K = J - 1
      L = J + 1
      A(K) = 1.
      A(L) = 1.
      A(J) = -10.
      K = J + 12
      A(K) = 4.
      N = N + 1
   15 CONTINUE
      M = 2
      N = 6
      DO 20 I = 112,168,14
      M = M + N
      J = I + M
      K = J - 1
      L = J + 1
      A(K) = 1.
      A(L) = 1.
      A(J) = -4.
      K = J + 12
      A(K) = 1.
      N = N + 1
   20 CONTINUE
      DO 25 I = 223,348,25
      J = I + 11
      K = I + 12
      L = I + 13
      M = I + 24
      A(I) = 4.
      A(J) = 1.
      A(K) = -10.
      A(L) = 1.
      A(M) = 4.
   25 CONTINUE
      DO 30 I = 523,648,25
      J = I + 11
      K = I + 12
      L = I + 13
      M = I + 24
      A(I) = 4.
      A(J) = 1.
      A(K) = -10.
      A(L) = 1.
      A(M) = 4.
   30 CONTINUE
      DO 35 I = 823,948,25
      J = I + 11
      K = I + 12
      L = I + 13
      M = I + 24
      A(I) = 4.
      A(J) = 1.
```

```
      A(K) = -10.
      A(L) = 1.
      A(M) = 4.
   35 CONTINUE
      DO 40 I = 2248,2373,25
      J = I + 11
      K = I + 12
      L = I + 13
      M = I + 24
      A(I) = 4.
      A(J) = 1.
      A(K) = -10.
      A(L) = 1.
      A(M) = 4.
   40 CONTINUE
      DO 45 I = 3023,3123,25
      J = I + 11
      K = I + 12
      L = I + 13
      M = I + 24
      A(I) = 1.
      A(J) = 4.
      A(K) = -10.
      A(L) = 4.
      A(M) = 1.
   45 CONTINUE
      DO 50 I = 3323,3423,25
      J = I + 11
      K = I + 12
      L = I + 13
      M = I + 24
      A(I) = 1.
      A(J) = 4.
      A(K) = -10.
      A(L) = 4.
      A(M) = 1.
   50 CONTINUE
      DO 55 I = 3623,3723,25
      J = I + 11
      K = I + 12
      L = I + 13
      M = I + 24
      A(I) = 1.
      A(J) = 4.
      A(K) = -10.
      A(L) = 4.
      A(M) = 1.
   55 CONTINUE
      DO 60 I = 3923,4023,25
      J = I + 11
      K = I + 12
      L = I + 13
      M = I + 24
      A(I) = 1.
      A(J) = 4.
      A(K) = -10.
      A(L) = 4.
      A(M) = 1.
   60 CONTINUE
      DO 65 I = 4223,4323,25
      J = I + 11
      K = I + 12
      L = I + 13
      M = I + 24
      A(I) = 1.
      A(J) = 4.
      A(K) = -10.
      A(L) = 4.
      A(M) = 1.
   65 CONTINUE
      DO 70 I = 4523,4623,25
      J = I + 11
```

```
      K = I + 12
      L = I + 13
      M = I + 24
      A(I) = 1.
      A(J) = 4.
      A(K) = -10.
      A(L) = 4.
      A(M) = 1.
   70 CONTINUE
      DO 75 I = 398,498,25
      J = I + 11
      K = I + 12
      L = I + 13
      M = I + 24
      A(I) = 1.
      A(J) = 1.
      A(K) = -4.
      A(L) = 1.
      A(M) = 1.
   75 CONTINUE
      DO 80 I = 698,798,25
      J = I + 11
      K = I + 12
      L = I + 13
      M = I + 24
      A(I) = 1.
      A(J) = 1.
      A(K) = -4.
      A(L) = 1.
      A(M) = 1.
   80 CONTINUE
      DO 85 I = 2148,2223,25
      J = I + 11
      K = I + 12
      L = I + 13
      M = I + 24
      A(I) = 1.
      A(J) = 1.
      A(K) = -4.
      A(L) = 1.
      A(M) = 1.
   85 CONTINUE
      DO 90 I = 2848,2973,25
      J = I + 11
      K = I + 12
      L = I + 13
      M = I + 24
      A(I) = 1.
      A(J) = 1.
      A(K) = -4.
      A(L) = 1.
      A(M) = 1.
   90 CONTINUE
      DO 95 I = 3148,3273,25
      J = I + 11
      K = I + 12
      L = I + 13
      M = I + 24
      A(I) = 1.
      A(J) = 1.
      A(K) = -4.
      A(L) = 1.
      A(M) = 1.
   95 CONTINUE
      DO 100 I = 3448,3573,25
      J = I + 11
      K = I + 12
      L = I + 13
      M = I + 24
      A(I) = 1.
      A(J) = 1.
      A(K) = -4.
```

```
      A(L) = 1.
      A(M) = 1.
  100 CONTINUE
      DO 105 I = 3748,3873,25
      J = I + 11
      K = I + 12
      L = I + 13
      M = I + 24
      A(I) = 1.
      A(J) = 1.
      A(K) = -4.
      A(L) = 1.
      A(M) = 1.
  105 CONTINUE
      DO 110 I = 4048,4173,25
      J = I + 11
      K = I + 12
      L = I + 13
      M = I + 24
      A(I) = 1.
      A(J) = 1.
      A(K) = -4.
      A(L) = 1.
      A(M) = 1.
  110 CONTINUE
      DO 115 I = 4348,4473,25
      J = I + 11
      K = I + 12
      L = I + 13
      M = I + 24
      A(I) = 1.
      A(J) = 1.
      A(K) = -4.
      A(L) = 1.
      A(M) = 1.
  115 CONTINUE
      DO 120 I = 2423,2523,25
      J = I + 11
      K = I + 12
      L = I + 13
      M = I + 24
      A(I) = 1.
      A(J) = 1.
      A(K) = -4.
      A(L) = 1.
      A(M) = 1.
  120 CONTINUE
      DO 125 I = 1048,1098,25
      J = I + 11
      K = I + 12
      L = I + 13
      M = I + 23
      A(I) = 1.
      A(J) = 1.
      A(K) = -4.
      A(L) = 1.
      A(M) = 1.
  125 CONTINUE
      DO 130 I = 1123,1248,25
      J = I + 11
      K = I + 12
      L = I + 13
      M = I + 23
      A(I) = 8.
      A(J) = 5.
      A(K) = -50.
      A(L) = 5.
      A(M) = 32.
  130 CONTINUE
      DO 135 I = 1398,1523,25
      J = I + 1
      K = I + 11
```

```
      L = I + 12
      M = I + 13
      N = I + 23
      A(J) = 16.
      A(K) = 1.
      A(L) = -34.
      A(M) = 1.
      A(N) = 16.
  135 CONTINUE
      DO 140 I = 1598,1648,25
      J = I + 1
      K = I + 11
      L = I + 12
      M = I + 13
      N = I + 23
      A(J) = 4.
      A(K) = 1.
      A(L) = -10.
      A(M) = 1.
      A(N) = 4.
  140 CONTINUE
      A(1661) = 0.
      DO 145 I = 1673,1798,25
      J = I + 1
      K = I + 11
      L = I + 12
      M = I + 13
      N = I + 23
      A(J) = 32.
      A(K) = 5.
      A(L) = -50.
      A(M) = 5.
      A(N) = 8.
  145 CONTINUE
      DO 150 I = 1948,2073,25
      J = I + 1
      K = I + 11
      L = I + 12
      M = I + 13
      N = I + 24
      A(J) = 4.
      A(K) = 1.
      A(L) = -10.
      A(M) = 1.
      A(N) = 4.
  150 CONTINUE
      DO 155 I = 2548,2673,25
      J = I + 11
      K = I + 12
      L = I + 13
      M = I + 24
      A(I) = 8.
      A(J) = 3.
      A(K) = -18.
      A(L) = 3.
      A(M) = 4.
  155 CONTINUE
      DO 160 I = 2723,2823,25
      J = I + 11
      K = I + 12
      L = I + 13
      M = I + 24
      A(I) = 2.
      A(J) = 3.
      A(K) = -9.
      A(L) = 3.
      A(M) = 1.
  160 CONTINUE
      N = 5
      M = 0
      DO 170 I = 4648,4743,19
      L = I + M
```

```
      J = L + 11
      K = L + 12
      A(L) = 1.
      A(J) = 1.
      A(K) = -4.
      J = L + 13
      A(J) = 1.
      M = M + N
      N = N - 1
  170 CONTINUE
      N = 3
      M = 0
      DO 175 I = 4795,4837,14
      L = I + M
      J = L + 11
      K = L + 12
      A(L) = 1.
      A(J) = 4.
      A(K) = -10.
      J = L + 13
      A(J) = 4.
      M = M + N
      N = N - 1
  175 CONTINUE
      A(1) = -10.
      A(2) = 1.
      A(13) = 4.
      A(99) = 1.
      A(100) = -9.
      A(101) = 2.
      A(112) = 3.
      A(211) = 0.
      A(234) = 0.
      A(373) = 3.
      A(384) = 1.
      A(385) = -9.
      A(386) = 2.
      A(397) = 3.
      A(511) = 0.
      A(534) = 0.
      A(673) = 3.
      A(684) = 1.
      A(685) = -9.
      A(686) = 2.
      A(697) = 3.
      A(811) = 0.
      A(834) = 0.
      A(973) = 3.
      A(984) = 1.
      A(985) = -9.
      A(986) = 2.
      A(997) = 3.
      A(998) = 1.
      A(1009) = 1.
      A(1010) = -4.
      A(1011) = 1.
      A(1022) = 1.
      A(1023) = 4.
      A(1034) = 3.
      A(1035) = -18.
      A(1036) = 3.
      A(1111) = 0.
      A(1134) = 0.
      A(1298) = 4.
      A(1309) = 3.
      A(1310) = -18.
      A(1321) = 8.
      A(1273) = 8.
      A(1284) = 2.
      A(1285) = -30.
      A(1286) = 4.
      A(1296) = 16.
```

```
A(1324) = 2.
A(1335) = -12.
A(1336) = 2.
A(1346) = 4.
A(1349) = 4.
A(1359) = 3.
A(1360) = -18.
A(1361) = 3.
A(1371) = 8.
A(1374) = 4.
A(1384) = 3.
A(1385) = -18.
A(1396) = 8.
A(1409) = 0.
A(1549) = 24.
A(1559) = 2.
A(1560) = -54.
A(1561) = 4.
A(1571) = 24.
A(1574) = 3.
A(1584) = 1.
A(1585) = -9.
A(1596) = 3.
A(1609) = 0.
A(1661) = 0.
A(1684) = 0.
A(1824) = 8.
A(1834) = 4.
A(1835) = -30.
A(1836) = 2.
A(1846) = 16.
A(1849) = 8.
A(1859) = 3.
A(1860) = -18.
A(1871) = 4.
A(1874) = 4.
A(1885) = -12.
A(1886) = 2.
A(1897) = 2.
A(1899) = 8.
A(1909) = 3.
A(1910) = -18.
A(1911) = 3.
A(1922) = 4.
A(1924) = 8.
A(1934) = 3.
A(1935) = -18.
A(1947) = 4.
A(1959) = 0.
A(2099) = 3.
A(2109) = 1.
A(2110) = -9.
A(2111) = 2.
A(2122) = 3.
A(2124) = 1.
A(2134) = 1.
A(2135) = -4.
A(2136) = 1.
A(2147) = 1.
A(2148) = 0.
A(2236) = 0.
A(2259) = 0.
A(2398) = 3.
A(2409) = 1.
A(2410) = -9.
A(2411) = 2.
A(2422) = 3.
A(2536) = 0.
A(2559) = 0.
A(2698) = 4.
A(2709) = 2.
A(2710) = -12.
```

```
      A(2711) = 4.
      A(2722) = 2.
      A(2836) = 0.
      A(2859) = 0.
      A(2998) = 3.
      A(3009) = 4.
      A(3010) = -18.
      A(3011) = 8.
      A(3022) = 3.
      A(3136) = 0.
      A(3159) = 0.
      A(3298) = 3.
      A(3309) = 4.
      A(3310) = -18.
      A(3311) = 8.
      A(3322) = 3.
      A(3436) = 0.
      A(3459) = 0.
      A(3598) = 3.
      A(3609) = 4.
      A(3610) = -18.
      A(3611) = 8.
      A(3622) = 3.
      A(3736) = 0.
      A(3759) = 0.
      A(3898) = 3.
      A(3909) = 4.
      A(3910) = -18.
      A(3911) = 8.
      A(3922) = 3.
      A(4036) = 0.
      A(4059) = 0.
      A(4198) = 3.
      A(4209) = 4.
      A(4210) = -18.
      A(4211) = 8.
      A(4222) = 3.
      A(4336) = 0.
      A(4359) = 0.
      A(4498) = 3.
      A(4509) = 4.
      A(4510) = -18.
      A(4511) = 8.
      A(4522) = 3.
      A(4636) = 0.
      A(4659) = 0.
      A(4777) = 3.
      A(4788) = 4.
      A(4789) = -18.
      A(4790) = 8.
      A(4857) = 1.
      A(4868) = 4.
      A(4869) = -10.
C
C     INPUT THE BOUNDARY CONDITIONS
C
      C(1) = -46.
      C(2) = -32.
      C(3) = -28.
      C(4) = -24.
      C(5) = -20.
      C(6) = -16.
      C(7) = -12.
      C(8) = -2.5
      C(9) = -2.
      C(10) = -1.5
      C(11) = -1.
      C(12) = -.5
      C(13) = -10.
      C(25) = -10.
      C(37) = -10.
      C(45) = -16.
```

```
      C(49) = -50.
      C(56) = -6.
      C(57) = -8.
      C(60) = -10.
      C(67) = -6.25
      C(68) = -3.125
      C(78) = -10.5
      C(79) = -14.
      C(90) = -3.5
      C(71) = -50.
      C(82) = -10.
      C(94) = -10.
      C(106) = -30.
      C(118) = -10.
      C(130) = -10.
      C(142) = -10.
      C(154) = -10.
      C(166) = -10.
      C(178) = -10.
      C(190) = -19.
      C(191) = -8.
      C(192) = -7.
      C(193) = -6.
      C(194) = -5.
      C(195) = -4.
      C(196) = -9.
      C(197) = -2.5
      C(198) = -2.
      C(199) = -1.5
      C(200) = -1.
      C(201) = -0.5
      DO 180 I = 1,201
      B(I,1) = C(I)
  180 CONTINUE
C
C     SOLVE THE TWO HUNDRED AND ONE EQUATIONS
C     SIMULTANEOUSLY TO OBTAIN A SOLUTION FOR THE
C     STREAM FUNCTION AT DISTINCT POINTS IN THE FLOW.
C
      CALL GELB(B,A,201,1,12,12,.001,IER)
      WRITE (6,900)
      DO 210 I = 1,201
      D(I) = B(I,1)
  210 CONTINUE
C
C     WRITE THE SOLUTION TO THE STREAM FUNCTION AT
C     EACH DISTINCT POINT ALLOWING FOR VARIABLE MESH
C     CONSIDERATIONS
C
      DO 220 I = 1,37,12
      J = I
      K = J + 11
      WRITE(6,400) (D(L),L=J,K)
      WRITE (6,300)
  220 CONTINUE
      DO 230 I = 49,71,11
      J = I
      K = J + 10
      WRITE(6,500) (D(L),L=J,K)
  230 CONTINUE
      WRITE (6,300)
      DO 240 I = 82,94,12
      J = I
      K = J + 11
      WRITE(6,400) (D(L),L=J,K)
      WRITE (6,300)
  240 CONTINUE
      DO 250 I = 106,190,12
      J = I
      K = J + 11
      WRITE (6,400) (D(L),L=J,K)
      WRITE (6,900)
```

```
250 CONTINUE
    STOP
    END
```

A sample output follows on the subsequent page. For this case, the flow velocity was evenly distributed in the canard augmentor and was constrained to be twice the velocity of freestream conditions.

Boundary conditions are not included in the output. The decimal point of each stream function value represents the approximate relative position of each solution point in the domain depicted in Figure 2.

9.01	8.01	7.02	6.04	5.06	4.13	3.51	2.71	2.10	1.56	1.04	0.52
9.01	8.03	7.05	6.07	5.11	4.18	3.33	2.73	2.15	1.60	1.07	0.53
9.02	8.04	7.07	6.10	5.15	4.22	3.28	2.72	2.15	1.63	1.10	0.55
9.02	8.05	7.09	6.13	5.19	4.26	3.30	2.72	2.10	1.67	1.15	0.58
9.03	8.06	7.10	6.15	5.22	4.30	3.37	2.78	—	1.82	1.24	0.62
9.03	8.06	7.10	6.15	5.22	4.32	3.44	2.87	—	1.99	1.30	0.64
9.03	8.07	7.11	6.16	5.23	4.33	3.53	3.03	—	2.22	1.34	0.65

9.03	8.07	7.11	6.15	5.22	4.313.44	2.99	2.60	1.99	1.30	0.64
9.03	8.06	7.10	6.15	5.21	4.283.37	2.89	2.41	1.85	1.24	0.62
9.03	8.06	7.10	6.14	5.19	4.243.30	2.81	2.30	1.75	1.18	0.59
9.03	8.05	7.08	6.12	5.15	4.183.20	2.69	2.18	1.65	1.10	0.55
9.02	8.05	7.07	6.09	5.11	4.133.13	2.62	2.11	1.59	1.06	0.53

9.02 8.04 7.05 6.07 5.08 4.093.09 2.58 2.07 1.56 1.04 0.52

9.01 8.03 7.04 6.05 5.06 4.063.06 2.55 2.05 1.54 1.03 0.51

9.01 8.02 7.03 6.04 5.04 4.043.04 2.53 2.03 1.52 1.02 0.51

9.01 8.01 7.02 6.02 5.03 4.033.02 2.52 2.02 1.51 1.01 0.50

9.00 8.01 7.01 6.01 5.01 4.013.01 2.51 2.01 1.51 1.00 0.50

LIST OF REFERENCES

1. NASA TN D-6394, Potential Flow Solution for a STOL Wing Propulsion System, by J. A. Albers and M. C. Potter, p. 10, July, 1971.

2. Spence, D. A., "The Lift on a Thin Airfoil with a Jet Augmented Flap, Aeronautics Quarterly, Volume 9, pp. 287-289, 1958.

3. AIAA Paper No. 73-652, A Jet-Wing Lifting Surface Theory Using Elementary Vortex Distributions, by C. C. Shen, M. L. Lopez, and N. F. Wasson, 6th Fluid and Plasma Dynamics Conference, pp. 3-4, 18 July 1973.

4. NASA CR-1774, Recirculation Characteristics of a Small-Scale, VTOL Lift Engine Pod, by G. R. Hall, pp. 30-31, May, 1971.

5. NASA TN D-7014, Reingestion Characteristics and Inlet Flow Distortion of V/STOL Lift-Engine Fighter Configurations, by J. V. Kirk and J. P. Barrack, p. 5, December, 1970.

6. NASA CR-1625, Scaling of VTOL Recirculation Effects, by G. R. Hall, p. 31, August, 1970.

7. NASA CR-1863, Model Tests of Concepts to Reduce Hot Gas Ingestion in VTOL Lift Engines, by G. R. Hall, pp. 1, 42-44, July, 1971.

8. Doryland, A. T., and Killian, J. E., Construction of One-Tenth Scale Model of the XFV-12A and Canard Performance Test, MS Thesis, Naval Postgraduate School, Monterey, California, 1974.

9. Powers, David I., Boundary Value Problems, pp. 45-46, 113, Academic Press, 1972.

10. Kip, Arthur F., Fundamentals of Electricity and Magnetism, pp. 87-88, 581, McGraw-Hill, 1962.

11. Malavaard, L., "Electrolytic Plotting Tank," Physical Measurements in Gas Dynamics and Combustion, Princeton Series on High Speed Aerodynamics and Propulsion, Volume IX, pp. 322-340.

12. NASA SP-116, Considerations for Revision of V/STOL Handling Qualities Criterion, by Seth B. Anderson, Conference on V/STOL and STOL Aircraft, p. 233, 5 April 1966.

13. NASA SP-83, Conference on Aircraft Operating Problems, by NASA Staff, May 1965.

14. AIAA Paper No. 74-1191, A Computer Program for Aircraft Thrust Ejector Analysis, by G. R. Salter, AIAA/SAE 10th Propulsion Conference, p. 8, 23 October 1974.

15. Reynolds, William C., and Perkins, Henry C., Engineering Thermodynamics, pp. 539-557, McGraw-Hill, 1970.

INITIAL DISTRIBUTION LIST

		No. Copies
1.	Defense Documentation Center Cameron Station Alexandria, Virginia 22314	2
2.	Library, Code 0212 Naval Postgraduate School Monterey, California 93940	2
3.	Department Chairman, Code 57 Department of Aeronautics Naval Postgraduate School Monterey, California 93940	2
4.	Distinguished Professor A. E. Fuhs, Code 57Fu Department of Aeronautics Naval Postgraduate School Monterey, California 93940	4
5.	2/LT C. L. Peterson, USMC P. O. Box 1000 Lebec, California 93243	3
6.	LCDR J. E. Killian, USN VA-174 Cecil Field Jacksonville, Florida 32212	1
7.	LT A. T. Doryland, USN 829 Squadron RNAS Portland Weymouth, Dorsett England	2
8.	Mr. R. F. Siewert, Code 320D Naval Air Systems Command Washington, D. C. 20360	2
9.	CAPTAIN R. L. Von Gerichten, USN VTOL Program Officer Naval Air Systems Command Washington, D. C. 20360	1
10.	CAPTAIN A. D. Williams, USN Code 536 Naval Air Systems Command Washington, D. C. 20360	1

11.	Dr. Brian Quinn A.R.L. Wright-Patterson AFB, Ohio 45433	1
12.	Mr. V. R. Hancock XFV-12A Program Manager Columbus Aircraft Division North American Rockwell 4300 East Fifth Avenue Columbus, Ohio 43216	1
13.	CAPTAIN A. A. Schaufelberger, USN Code PDMA-1 Naval Air Systems Command Washington, D. C. 20360	1
14.	Mr. John Tankersley Columbus Aircraft Division North American Rockwell 4300 East Fifth Avenue Columbus, Ohio 43216	1
15.	Mr. Robert M. Williams Aviation and Surface Effects Department Naval Ship Research and Development Center Bethesda, Maryland 20034	1

Thesis
P4124 Peterson
c.1
160072
Flow visualization
studies of the XFV-12A.